

---

---

STRUCTURE, PHASE TRANSFORMATIONS,  
AND DIFFUSION

---

---

## MgB<sub>2</sub>-Based Superconductors: Structure and Properties

T. P. Krinitsina<sup>a</sup>\*, E. I. Kuznetsova<sup>a</sup>, M. V. Degtyarev<sup>a</sup>, and Yu. V. Blinova<sup>a</sup>

<sup>a</sup> M.N. Miheev Institute of Metal Physics, Ural Branch, Russian Academy of Sciences, Ekaterinburg, 620108 Russia

\*e-mail: krinitsina@imp.uran.ru

Received July 5, 2021; revised August 8, 2021; accepted August 16, 2021

**Abstract**—A brief review of synthesis methods of MgB<sub>2</sub> and the effect of alloying and thermomechanical treatment on the structure and properties of MgB<sub>2</sub> is presented. The review observes the production methods of MgB<sub>2</sub>-based wires and cables and their applications and perspectives of potential use. Deposition methods of MgB<sub>2</sub> films and on the possibility of application of MgB<sub>2</sub> films in electronics and for fundamental research in the condensed-matter physics are reported on.

**Keywords:** magnesium diboride, alloying, critical current, superconductivity

**DOI:** 10.1134/S0031918X2112005X

### INTRODUCTION

The superconductivity of the MgB<sub>2</sub> magnesium diboride was discovered in January, 2001, by Japanese scientist J. Akimitsu from the Aoyama Gakuin University; this information was published in *Nature* in March 1, 2021 [1]. The superconducting transition temperature,  $T_c$ , of MgB<sub>2</sub> is ~40 K and is the highest temperature for low-temperature superconductors. The crystal structure of MgB<sub>2</sub> is formed by alternating layers of boron and magnesium atoms. The lattice parameters of the hexagonal unit cell are  $a = 3.086$  and  $c = 3.524$  Å [1]. It was confirmed that the finding was to some extent occasional [2–4]; however, the interest that was aroused by the finding was great. Already seven months after the information about the superconductivity of MgB<sub>2</sub>, the results of more than 260 studies of this superconductor were reported in the conference in Sendai (Japan). Works were started in laboratories around the world, which resulted in a huge increase in the number of reports about various properties of MgB<sub>2</sub>. They covered the isotopic effect [6], thermodynamic and transport properties [7], band structure of energy states [8, 9], critical current density [10, 11], and alloying [12] and pressure [13] effects. The initial agiotage was mainly based on the fact that, first, MgB<sub>2</sub> is the simple intermetallic compound of two inexpensive elements. Second, in contrast to the superconductivity of cuprate high-temperature superconductors (HTSCs), the superconductivity of the compound is realized via the traditional electron–phonon coupling mechanism. The prospects of application of MgB<sub>2</sub> in practice seemed to be more promising as compared to those of HTSCs even despite the fact that  $T_c = 40$  K is substantially lower than  $T_c = 160$  K observed in HTSCs. The

most direct evidence of the phonon mechanism is the isotropic effect, according to which the decrease in  $T_c$  with increasing isotropic mass of the superconductor indicates the lattice participation in the superconductivity [14]. The BCS mechanism was also confirmed by photoemission spectroscopy [15], scanning tunnel microscopy [16], and neutron scattering measurements [17].

What is so remarkable about MgB<sub>2</sub> that has attracted the attention of scientists around the world? Already since the finding, it became clear that its properties are unique from the viewpoint of physics, and MgB<sub>2</sub> is not a common superconductor. Usually, a superconductor at a temperature below  $T_c$  is characterized by the existence of a single temperature-dependent energy gap  $\Delta(T)$  such that, in order to split a Cooper pair into two quasiparticles, the minimum energy  $2\Delta(T)$  is required. The MgB<sub>2</sub> compound is characterized by two such gaps; one of them has  $\Delta(0) \sim 2$  meV, and the other has  $\Delta(0) \sim 7$  meV [2, 18]. Both the gaps obey the temperature dependence predicted by BCS theory and disappear at the same temperature  $T_c$ . According to the BCS theory,  $2\Delta(0) = 3.53 kT_c$  [14]. In this case, two energy gaps, be they independent, should correspond to two  $T_c$  temperatures that are 15 and 45 K, respectively [19]. However, the interelectron interaction determines the existence of coupling between two gaps, which leads to the same  $T_c$  close to 40 K.

Both these gaps appear owing to the existence of two energy bands,  $\sigma$  and  $\pi$ , in which boron atoms are located [9]. According to data of [20], the  $\sigma$ – $\pi$  interband electron scattering with impurities is extremely low mainly because of differences in the symmetry of their charge-density distributions. This low interband

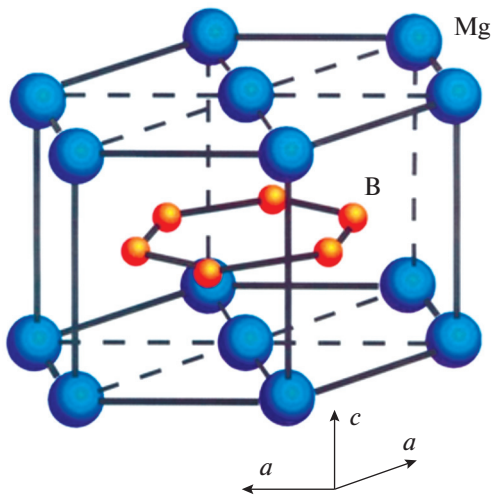


**Fig. 1.** Structure of  $\text{MgB}_2$  containing graphite-like B layers separated with hexagonal close-packed Mg layers [5].

scattering distinguishes  $\text{MgB}_2$  from the other superconductors with several energy bands, in which the interband scattering usually blurs the immanent characteristics of bands.

The existence of two energy gaps was found quickly and confirmed by many experiments, which include measurements of the specific heat [21, 22], point-contact spectroscopy [23], photoemission spectroscopy [24], and scanning tunnel microscopy (STM) [25]. Studies performed with thin films also played their part in the observation of two energy gaps. For example, two different energy gaps that disappear at the same  $T_c$  were found for  $\text{MgB}_2$  thin films by tunnel spectroscopy [26]. According to data of [27], the spectra of two energy bands depend on tunneling directions. The existence of two gaps (two superconducting order parameters) in  $\text{MgB}_2$  with their inherent Josephson coupling and phase difference [28] leads to new effects that do not exist in single-gap superconductors. For example, in  $\text{MgB}_2$ , the collective excitation corresponding to small fluctuations of the phase difference between two order parameters or the so-called Leggett mode can exist. There is a number of assumptions that the observed Leggett mode can be reached with thin-film  $\text{MgB}_2$ -based devices, such as Josephson transitions in  $\text{MgB}_2$  [29], Andreev contacts, and Josephson transitions between  $\text{MgB}_2$  and a superconductor with a single energy band [30, 31].

The two-band superconductivity model was first suggested in the end of the 1950s [32]; however,  $\text{MgB}_2$  is the first superconductor for which two-gap effects are pronounced [2, 19]. Problems related to the two-band superconductivity are discussed in detail in [14].

Along with the high  $T_c$  temperature of  $\text{MgB}_2$  that is  $\sim 40$  K, it has the simple crystal lattice, high coherence length, high critical current density, very low residual

resistance, and relatively low cost of starting components used for the synthesis. All these factors make  $\text{MgB}_2$  very attractive for the application in superconductors, in particular, in electronics.

In this review, synthesis methods of  $\text{MgB}_2$ , the effect of alloying and thermomechanical treatment on the structure and properties of  $\text{MgB}_2$ , and production methods for  $\text{MgB}_2$ -based wires are considered. Prospects of application of  $\text{MgB}_2$ -based wires and cables for power lines are also discussed. Moreover, the principles of  $\text{MgB}_2$  film growth and successful deposition methods used for the preparation of  $\text{MgB}_2$  films and possibility of applying  $\text{MgB}_2$  films in electronics as well are reported in this work.

## SYNTHESIS AND CRYSTAL STRUCTURE OF $\text{MgB}_2$ AND SUPERCONDUCTORS BASED ON IT

### *Crystal Structure of $\text{MgB}_2$*

The magnesium diboride classified among layered binary compounds, has a simple  $\text{AlB}_2$ -type hexagonal structure (space group  $P6/mmm$ ), which is typical of diborides (Fig. 1). Boron atoms in the crystal lattice form graphite-like layers that are arranged one above the other without shifting and are separated by hexagonal closed-packed planes of magnesium atoms. Boron atoms are arranged at the centers of trigonal prisms, vertexes of which are occupied with magnesium atoms. Borides of Mg, Al, Ti, Zr, Hf, V, Nb, Ta, Cr, Mo, W, V, Fe, and rare-earth metals crystallize with the formation of this structure type, which also is called the  $\text{AlB}_2$  aluminum boride structure type.

According to X-ray diffraction data available in numerous studies, the lattice parameters of  $\text{MgB}_2$  at room temperature are  $a = 3.08$  and  $c = 3.52$  Å. Insignificant differences in the lattice parameters can be related to manufacturing peculiarities and preparation conditions of this compound.

### *Methods of Synthesis of Magnesium Diboride*

Since the discovery of the superconductivity in  $\text{MgB}_2$ , hundreds of studies were carried out in the fields of both manufacturing technology and investigation of the characteristics of superconductors based on this compound. Much of the results of these studies are observed in reviews [5, 33–35].

Methods most widely used for manufacturing the magnesium diboride-based superconductors are the “powder in tube” (in situ and ex situ) and “magnesium diffusion” [36]. The production methods of composite magnesium diboride-based superconductors and the advantages and disadvantages of the methods are considered in the next chapter related to the production of  $\text{MgB}_2$  wires.

To directly prepare the MgB<sub>2</sub> compound, there are several widely used methods present in any modification; these are the pulsed laser deposition (of film), infiltration, direct synthesis of powders (bulk samples), thermal explosion, and high-temperature high-pressure synthesis of single crystals. Each of the processes has its own advantages and disadvantages with respect to both the properties of materials and developing the used technology. Despite the variety, all the methods assume the occurrence of solid-phase reaction between Mg and B. The majority of studies of bulk MgB<sub>2</sub> samples deal with the material prepared from reacted Mg and B powder mixture (direct synthesis of powders). In this case, the stoichiometric mixture of a B powder with micron-sized particles and a Mg powder (Mg + 2B) is placed in a hermetically sealed tube and is annealed at 800–1000°C and higher for a long time in an argon atmosphere [10, 37]. Since Mg is the highly volatile element, it is reasonable to perform annealing in sealed ampules under a high inert gas pressure. Figure 2 shows the phase diagram of the Mg–B system [38]. The compounds that are stable at room temperature and are well understood are MgB<sub>2</sub>, MgB<sub>4</sub>, and MgB<sub>7</sub> [39, 40].

Authors of work [41] selected three stages of the formation of the MgB<sub>2</sub> polycrystalline phase within different sintering temperature ranges, which preset the synthesis conditions and lead to corresponding superconducting properties. Initially, the MgB<sub>2</sub> phase appears at ~530°C in the microscopic scale and, after that, macroscopic areas appear within a narrow temperature range from 653 to 660°C; in this case, some amounts of residual magnesium and boron remain to a temperature of 700°C. The optimum temperature range of sintering to form the MgB<sub>2</sub> phase is determined to be from 750 to 900°C.

When studying the effect of the synthesis temperature on the grain size and grain-boundary morphology, which, in turn, affect the superconducting properties of a bulk sample, it was found that the best transport properties ( $J_c = 10^4$  A/cm<sup>2</sup> at 4 T) are ensured by the synthesis at 950°C [42].

There are experimental data in [43, 44], which indicate that one of the mechanisms of the formation of the MgB<sub>2</sub> phase at high temperatures (~1000°C) is the liquid-phase mechanism, according to which solid boron dissolves in liquid magnesium and, after reaching the composition close to the stoichiometry, the formation of MgB<sub>2</sub> crystals starts. This mechanism explains the observation of layered and “dendrite-like” structures in this compound in assuming that dense areas result from the primary solidification, whereas the loose areas contain secondary solidification products and impurity phases (Fig. 3).

Since results of many studies definitely indicate the possible losses of Mg in the course of the reaction between Mg and B at high temperatures, the low-temperature synthesis of MgB<sub>2</sub> is far more interesting from

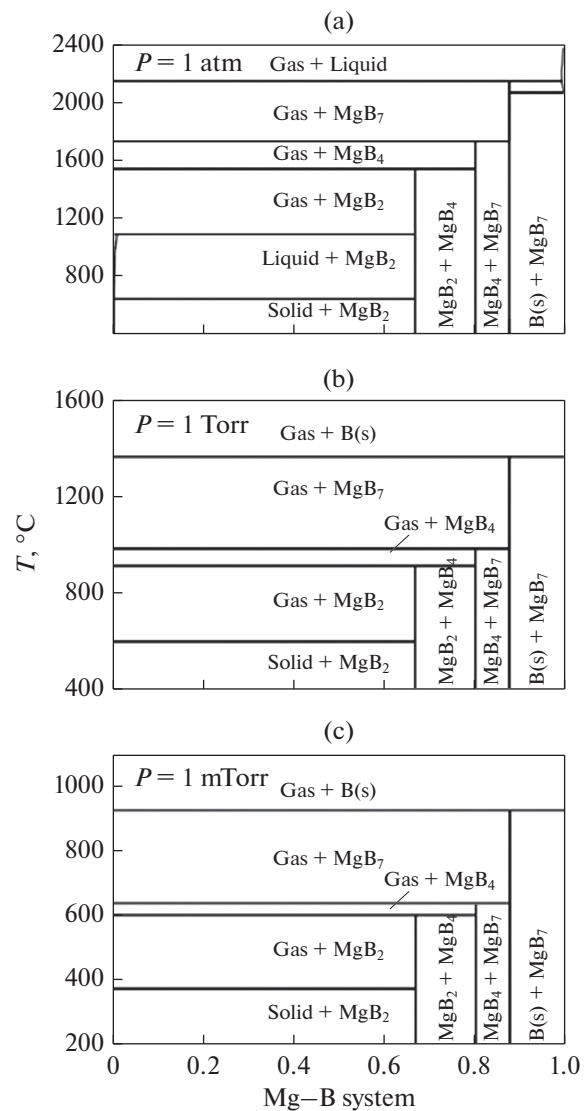
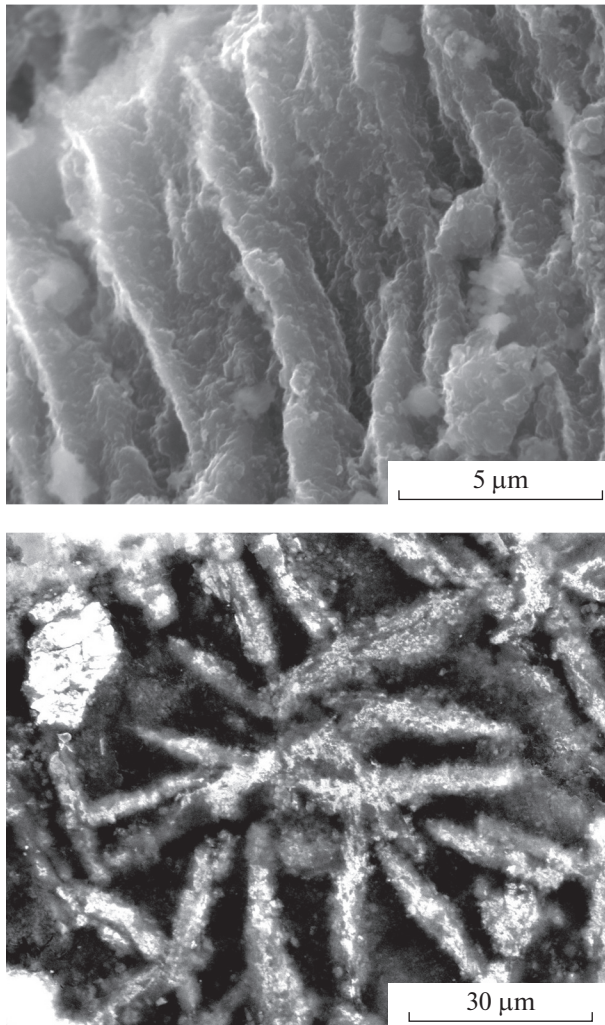


Fig. 2. Temperature—composition Mg–B phase diagrams at pressures of (a) 1 atm, (b) 1 Torr, and (c) 1 mTorr [38].

the viewpoint of the increase in  $J_c$  owing to improving both the grain coupling (increase in the density) and flux pinning [45].

A number of studies are focused on searching for methods for increasing the critical current density and improvement of the structure of bulk MgB<sub>2</sub> superconductors at the expense of optimization of sintering conditions. The use of two-stage sintering (at 775°C for 3 h in a pure argon atmosphere and subsequent sintering at 660°C for 24–100 h) showed that all samples subjected to repeated sintering are single-phase and characterized by an abrupt superconducting transition with  $T_c = \sim 37$  K. In this case,  $J_c$  increases as the time of repeated sintering increases (the maximum critical current density  $J_c = 170$  kA/cm<sup>2</sup> at 20 K was observed in a sample repeatedly sintered at 660°C for 100 h) [46].



**Fig. 3.** Layered structure (SEM) of a dense area in a  $\text{MgB}_2$  sample and dendrite-like structure (SEM image, secondary electron mode) of  $\text{MgB}_2$  [44].

The main disadvantage of the direct synthesis of powders consists in the fact that the high density of the prepared compound cannot be reached. In part, this is related to limitations upon mechanical densification of the initial powder mixture; even at the maximally possible density of the  $\text{Mg} + \text{B}$  mixture, the porosity of the synthesized ceramics anyway is high. This disadvantage does not take place in the case of synthesis methods called reactive infiltration of liquid magnesium; the essence of the method consists in the impregnation of preliminarily formed porous skeleton, which is formed from the more refractory component, with the molten low-melting component. In [47, 48], a boron powder was placed in an iron tube around a solid magnesium rod. After that, the iron tube was welded and heated at  $900^\circ\text{C}$  for 1 h. Magnesium melts and reacts with boron to form the high-density  $\text{MgB}_2$  compound. Moreover, the infiltration method is unique since it allows one to produce dense big configurations having a complex geometry, which are difficult to prepare by traditional sintering methods [49]. Figure 4 shows the schematic diagram of the synthesis process of massive  $\text{MgB}_2$  samples by the infiltration method [49].

The undesirable evaporation of magnesium during synthesis of  $\text{MgB}_2$  can be substantially suppressed and the material with the best functional characteristics and a density of  $\sim 98\%$  of the theoretical value can be obtained using high-pressure engineering [50–52].

One more method used for the fabrication of the  $\text{MgB}_2$  compound is the synthesis of the  $\text{Mg} + 2\text{B}$  mixture under thermal explosion conditions. Impurity oxygen is assumed to be the substantial factor that affects the kinetics and mechanism of the  $\text{MgB}_2$  formation. In the course of the synthesis under thermal explosion conditions at a heating rate exceeding  $150 \text{ deg/min}$ , the oxide film does not have time to be formed on the surface of magnesium particles; as a result, the reaction  $\text{Mg} + 2\text{B} \rightarrow \text{MgB}_2$  occurs via the

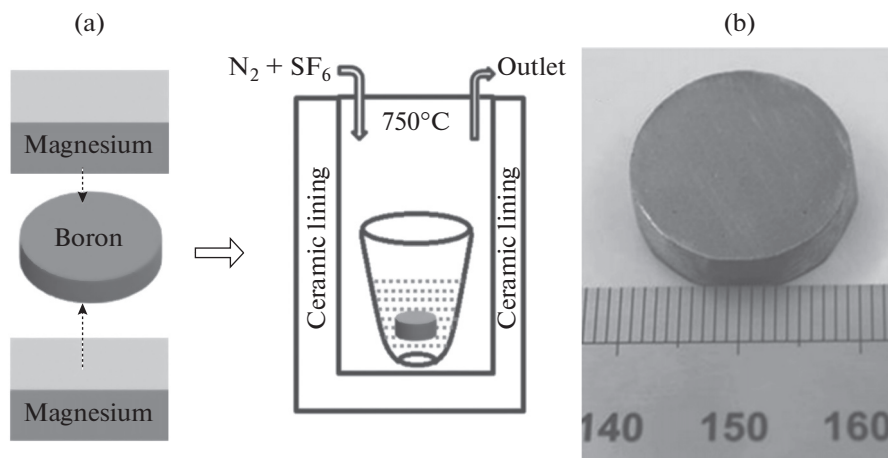


**Fig. 4.** (a) Schematic diagram of infiltration and growth and (b) appearance of  $\text{MgB}_2$  disk prepared by the method [49].

mechanism of reaction diffusion, and the spontaneous ignition temperature of the mixture was found to be below the melting temperature of magnesium [53–55].

Upon synthesis of the MgB<sub>2</sub> compound, special attention is paid to the size and morphology of initial powder particles and their chemical purity since it determines the compactibility, sintering ability, and service properties of the material. It was noted in a number of studies that, along with the temperature, pressure, and time of sintering, the quality and morphology of initial powder affect the sintering mechanism [56, 57]. The problem consists in the fact that the sufficiently wide ranges of the purity and sizes of used powders exist, and, unfortunately, their characteristics are not always discussed in detail in the literature; this makes difficult the estimation of the structure and properties achieved in published works.

One more serious problem of the MgB<sub>2</sub> compound prepared from the mixture of Mg and B powders is the above mentioned problem of contamination with secondary phases, in particular, MgO that, on the one hand, undoubtedly is the limiting factor for  $J_c$ . On the other hand, the effect of magnesium oxide on the properties of MgB<sub>2</sub> depends on the size and location of inclusions. When MgO particles are not located at grain boundaries, which is typical of the synthesized MgB<sub>2</sub>, and are uniformly distributed within grains, nanosized MgO inclusions can be considered as efficient pinning centers [58]. Authors of works [59, 60] assume that MgO, Mg(B<sub>2</sub>O<sub>3</sub>)<sub>2</sub>, and higher boride nanoinclusions are adequate pinning centers and favor reaching the high values of  $J_c$ .

Thus, to prepare the superconductors with the high critical current density, it is necessary not only to develop optimal synthesis conditions, but also to select the subsequent thermomechanical treatment conditions that ensure the optimum amount of pinning centers (grain boundaries, nanoparticles, etc.). To form the corresponding structure, various methods of cold and hot deformation are used [61, 62]. As a result of cold deformation under a high pressure in a “toroid” chamber and on Bridgman anvils and subsequent annealing of deformed samples, the critical current density was increased by three times as compared to that in the initial state (to  $6.7 \times 10^4$  A/cm<sup>2</sup> at 30 K) [63]. Moreover, the use of high pressures leads to the fact that the magnesium oxide and higher magnesium borides are present in the structure of the MgB<sub>2</sub> compound in the form of fine inclusions 10–70 nm in size, which act as the pinning centers [64]. In [65], the structure of bulk MgB<sub>2</sub> compound subjected to upset at room temperature and subsequently annealed at 650°C was studied. The obtained material is characterized by the dense nano-sized structure of the MgB<sub>2</sub> matrix phase with adequate intergrain coupling and uniform distribution of fine MgO inclusions ~10 nm in size (Fig. 5).

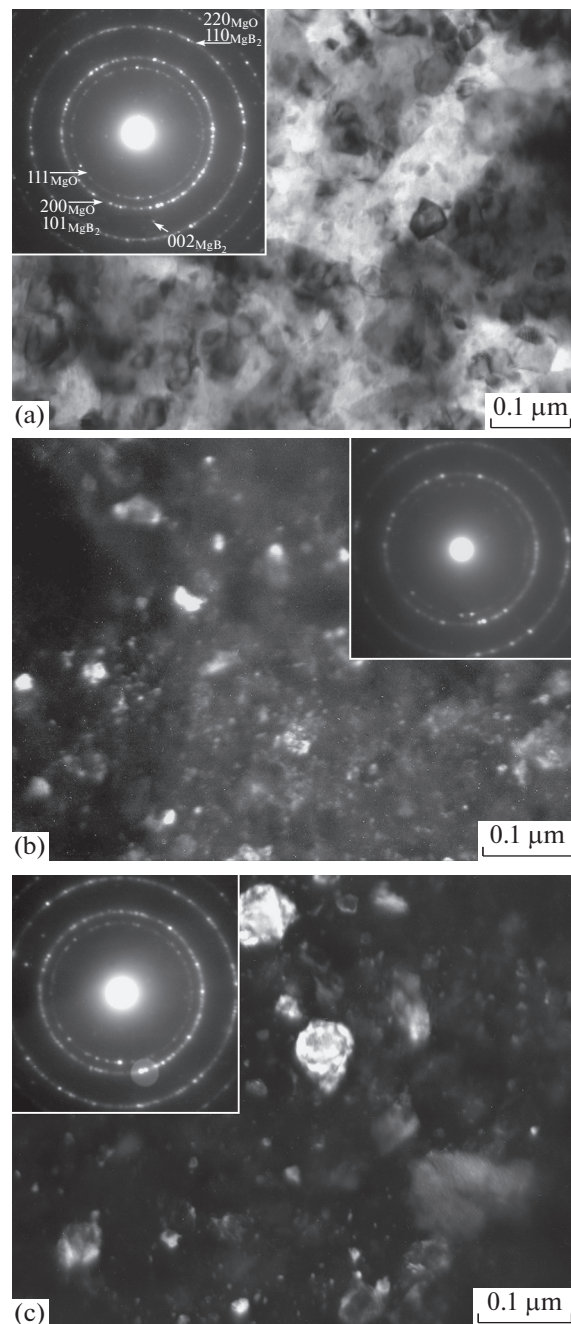


**Fig. 5.** TEM images of the structure of MgB<sub>2</sub> ceramics after reduction ( $P = 6.5$  GPa) and annealing at 750°C for 1 h: (a) bright-field image and ring electron-diffraction pattern; (b) dark-field image taken in (111)<sub>MgO</sub> marked with aperture; and (c) dark-field image taken in reflections (101)<sub>MgB<sub>2</sub></sub> and (200)<sub>MgO</sub> marked with aperture diaphragm [65].

### Alloying

In order to increase the critical currents, which the MgB<sub>2</sub>-based superconductor can have, the alloying as the alternative way is used in order to introduce defects. Alloying element atoms occupy either Mg or B

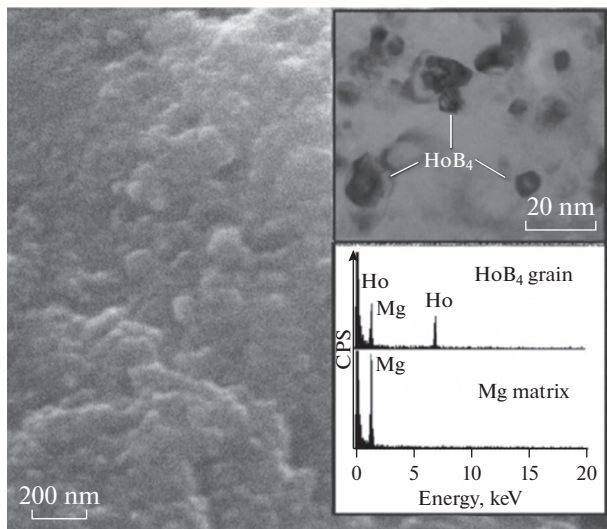


**Fig. 6.** Micrograph (SEM image) of  $\text{MgB}_2$  alloyed with 3.0%  $\text{Ho}_2\text{O}_3$ . Upper inset is micrographs and bottom inset is EDX spectra for nanoparticles shown in the micrograph (TEM) [75].

sites; therefore, it is of importance to know the location of alloying element atoms in order to determine the role of alloying elements in increasing the critical current density ( $J_c$ ). The positive effect on the increase in  $J_c$  in the  $\text{MgB}_2$  ceramics is observed, in particular, in alloying with carbon in the form of carbon nanotubes, nanodiamond, and other carbon-containing additions, for example, such as SiC [66–68]. Metallic additions, in particular, Ag, Ti, Ta, Zr [68–70] can also lead to a substantial increase in  $J_c$ .

The improvement of superconducting characteristics of a bulk composite ( $\text{MgB}_2$ -nano-diamond powder) additionally alloyed with Ag was demonstrated in [68]. It was found that AgMg nanoparticles introduced into the matrix are efficient pinning centers. The ceramics alloyed with 4.0 wt % Ag exhibits the highest value  $J_c = 389 \text{ kA/cm}^2$  at 20 K. It was reported in [71] that the  $\text{MgB}_2$  ceramics alloyed with carbon, which was prepared by infiltration with  $\text{B}_4\text{C}$  and SiC used as the carbon sources, contains the  $\text{Mg}(\text{B}_{1-x}\text{C}_x)_2$  and  $\text{B}_4\text{C}$  phases and exhibits the substantial increase in  $J_c$ , in particular at the lower temperature and in higher fields. Detailed microscopic studies of the effect of alloying with carbon during heat treatment of  $\text{MgB}_2$ -based wire (wires were sintered at  $650^\circ\text{C}$  for 30 min in a high-purity argon atmosphere) were performed in [72]. The authors have found that the magnesium vapor enters into boron shielded with carbon and forms nanocrystalline  $\text{MgB}_2$ -phase nuclei. After that, the growth of these particles and their merging take place. In this case, carbon atoms are forced out of  $\text{MgB}_2$  phase grains; however, a small amount of residual carbon generates the formation of stacking faults, which is accompanied by lattice distortions. Thus, the

authors conclude that the alloying with carbon leads to the appearance of crystal imperfection and improvement of superconducting properties. Moreover, it is noted that carbon prevents the boron agglomeration; as a result, the dense superconducting core of the wire forms.

In [70], it is reported about the investigation of bulk  $\text{MgB}_2$  superconductors alloyed with 10 at % Ti ( $T_c = 36.54 \text{ K}$ ) and 10 at % Zr ( $T_c = 37.10 \text{ K}$ ). The upper critical field for samples alloyed with the above metals, which was determined by the resistive method and extrapolated to 0 K, is 28 T. The upper field is substantially higher than that for the unalloyed  $\text{MgB}_2$  ( $\sim 20 \text{ T}$  at 0 K). The irreversibility fields are substantially higher than that for pure  $\text{MgB}_2$  and reach, for example, for  $\text{MgB}_2$  with 10 at % Ti, 15 T at 7.5 K. The critical current densities increase by 2 times and more at 20 K as compared to that for pure  $\text{MgB}_2$ . Moreover, in this study, results obtained after neutron irradiation of samples which indicate the substantial improvement of their transport properties, in particular, at low temperatures and in high magnetic fields, are reported. The authors note that the alloying of  $\text{MgB}_2$  with titanium and zirconium increases the upper critical field, irreversibility fields, and critical current densities, whereas the transition temperature slightly decreases. Defect structures that result from the neutron irradiation also are efficient and lead to almost identical results whatever the fact that the material is alloyed with Ti and Zr or unalloyed. The alloying effect of these additions on the superconducting properties and microstructure of sintered bulk  $\text{MgB}_2$  materials was studied in [73]. It was found that Ti and Zr produce beneficial effect on the sintering process, which manifests itself in improving the grain coupling. Bulk samples of  $\text{MgB}_2$  ceramics alloyed with Ti were synthesized, in the structure of which fine particles 10 nm in size were observed, and the high value of  $J_c$  was reached; it is more than  $1 \text{ MA/cm}^2$  at 0 T and 20 K. The authors relate the increase in  $J_c$  to the very good intergrain coupling and high density of pinning centers, which is formed by grain boundaries and MgO nanoparticles.

Polycrystalline  $\text{MgB}_2$  samples alloyed with Ti, Zr, and Hf [74] were fabricated by hot pressing method; the samples showed the increase in the critical current density from  $1.9 \times 10^5 \text{ A/cm}^2$  (0% Ti) to  $5.6 \times 10^5 \text{ A/cm}^2$  (5 at % Ti) in the eigenfield at 10 K.

Some difficulties in synthesizing the alloyed  $\text{MgB}_2$  compound were noted in a number of studies. Many of the elements selected as impurities form their own borides. For example, rare-earth metal oxides do not substitute for Mg and B atoms. The substitution could lead to lattice distortions and, therefore, changes in the lattice parameter; instead, the metals react with Mg and B with the formation of rare-earth borides. When the borides are formed in the form of nanosized precipitates within  $\text{MgB}_2$  grains (Fig. 6), they act as

pinning centers and increase  $J_c$  [75, 76]. The effect of additions of graphite oxide and oxides of a number of rare-earth metals (Re = La, Sm, Eu, Gd, Tb, and Ho) on the superconducting properties of MgB<sub>2</sub> are considered in [77]. It was shown that the critical current density and upper critical field substantially increase in alloyed samples; in this case, the critical temperature,  $T_c$ , is almost unchanged. In this work, different mechanisms of the magnetic flux pinning in alloyed samples were studied; it was found that the point pinning is the dominant mechanism in samples with the added graphite oxide, whereas the pinning at grain boundaries is the dominant mechanism in samples prepared with adding rare-earth metals.

Thus, during heat treatment, ReO reacts with Mg and B and forms nanosized ReB<sub>x</sub> inclusions. When these inclusions are located at MgB<sub>2</sub> grain boundaries, they act as the growth inhibiting substance and decelerate the MgB<sub>2</sub> grain growth; as the inclusions are present within grains, they have corresponding nanoscale sizes and can act as flux pinning centers. Thus, both the effects, namely, the grain refining and generation of additional pinning centers favor the increase in  $J_c$  [78].

In all the considered studies, the alloying with rare-earth oxides positively affects the MgB<sub>2</sub> compound (the alloying was considered by authors as relatively uniform); however, it is sufficiently difficult to relate the changes in the superconducting properties with additions of alloying impurities when a sample is inhomogeneous. In particular, the inhomogeneous distribution of an alloying addition can lead to the fact that some range of  $T_c$  can be observed due to the impurity concentration. In [79], MgB<sub>2</sub> single crystals were grown by the high-pressure method. The substitution of aluminum for magnesium in the single crystals leads to the stepped decrease in  $T_c$ , which indicates the possible appearance of phases characterized by different  $T_c$ .

The considered technologies demonstrate the main directions in developing the production methods of the magnesium diboride; however, the comprehensive pattern is not suggested. In particular, many applied approaches are directly related to the creation of concrete superconducting structures and devices, which are considered in individual sections of the review.

#### MgB<sub>2</sub>-BASED WIRES AND CABLES: MANUFACTURE AND APPLICATION

Articles based on the MgB<sub>2</sub> superconductor are produced in the form of thin films, ribbons, and wires for the application in electronics, in magnetic and electrotechnical devices. Let us consider the prospects of application of MgB<sub>2</sub> wires.

#### *Application of MgB<sub>2</sub> Conductors*

Magnesium diboride-based superconductors are mainly used for the creation of magnetic systems of medical tomographs, electric motors, and generators [80, 81]. The first industrial application of MgB<sub>2</sub> is the magnetic resonance imaging systems based on the MgB<sub>2</sub> ribbon, which are developed in ASG Superconductors (Leading Superconducting Technology, Columbus Superconductors, which is a world leader in advanced manufacturing technologies of long wire MgB<sub>2</sub>-based superconductors), and Paramed (Laser Technology Center for Medicine). To 2017, 28 systems are operated in hospitals and clinics around the world. Their manufacture has required the 18-km multifilamentary MgB<sub>2</sub> ribbon produced by ex situ method [82]. MgB<sub>2</sub> magnetic resonance imaging magnets are designed for the diagnostics of osteoporosis [83] and scanning of the human brain [84].

In fact, the MgB<sub>2</sub> superconductors have been ready, for several years, for application in power engineering, but are still not used on a large scale. Currently, the application of MgB<sub>2</sub> is limited mainly by demonstration and special-purpose applications in low (<5 T) magnetic fields and at temperatures to 15–20 K. Unfortunately, MgB<sub>2</sub> cannot always compete with HTSCs, such as cuprate superconductors (BSCCO-2223) and rare-earth barium-copper oxides (ReBCO) in fields in which liquid nitrogen cooling is beneficial. When the cost and electric characteristics of industrial MgB<sub>2</sub> wires at 15–20 K in medium and low fields become comparable with the characteristics and cost of Nb–Ti at 4.2 K, MgB<sub>2</sub> could substitute for Nb–Ti.

In Japan, in terms of a project related to the importation of a great amount of liquid hydrogen by shipping from Australia, an MgB<sub>2</sub>-based detector equipped with an external heater was designed. The detector, owing to good dynamic characteristics, can be used for measuring the tilting of the free surface of transported liquid upon rolling of the transporting ship. In the course of the experiment, synchronous measurements of the liquid level, temperature, pressure, ship traffic and accelerations, and tests for quick depressurization were performed [85, 86].

The most valuable solution of the problem related to the high energy flux transfer (dozens and hundreds of GW) for long distances (thousands kilometers) is “hybrid” hydrogen energy mains, in which, along with transportation of liquid hydrogen by a cryogenic main, the energy transfer by superconducting dc cables is realized. It is known that hydrogen is classified among the most efficient energy carrier, has the highest energy density among the other fuels, and exhibits good cooling properties in the liquid state. The evaporation heat of boiling hydrogen is 446 kJ/kg, whereas the evaporation heat of liquid helium and nitrogen is 20.28 and 199.1 kJ/kg, respectively. “Free of charge”

chill in hydrogen flow allows one to use superconducting cables in cryogenic mains for the electricity transmission, which substantially increase the energy flux transmission density [87]. For the first time, an experimental sample for the hybrid electric main was created in Russia in 2011 by a team of scientists from the Institute of Nanotechnologies of Microelectronics, Russian Academy of Scientists, All-Russian Scientific Research and Development Cable Institute, and Moscow Aviation Institute [81].

The European Project “Space Radiation Superconducting Shield” (SR2S) is aimed at developing a large superconducting toroidal magnet intended for protecting the human environment against the cosmic ionized irradiation during prolonged cosmic flights. In designing this magnet,  $MgB_2$  conductors with a titanium coating were used [88, 89].

Currently, the superconducting high-current lines supplying superconducting magnets in super-power High-Luminosity Large Hadron Collider (HL-LHC), which are developed in CERN (European Organization for Nuclear Research), is the most attractive applied project for  $MgB_2$  in the world. The  $MgB_2$  cables comprised the assemblage, each of which is  $\sim 100$  m long and carries a current of 18 kA, are fabricated from round  $MgB_2$  conductors with a total permissible output current capacity of  $\sim 150$  kA at 20 K [90]. The development of round  $MgB_2$  conductor, which is more suitable for the assemblage and has electric characteristics and mechanical properties that allow one to use the conductor in high-current cables, was started in cooperation with CERN and Columbus Superconductors. The ex situ conductor is 1 mm in diameter. It consists of 37 superconducting filaments, each of which has an equivalent diameter of  $\sim 60$   $\mu m$ ; the filaments are twisted at a pitch of 100 mm. The  $MgB_2$  filaments fabricated from a high-purity boron powder are surrounded by a niobium barrier and integrated in a nickel core. The Monel matrix surrounding the core is covered with copper and the copper surface is covered with tin. The cable structure is described in detail in [91]. The “Columbus Superconductors” has fabricated 80 km of wires and delivered them to CERN by pieces more than 500 m in length. Hundreds of measurements performed in CERN and “Columbus Superconductors” using short wire samples confirmed the uniformity and correspondence of electric characteristics, for which a minimum critical current of 186 A at 25 K and 0.9 T is required. The in-depth study of mechanical characteristics of wires and cables made from twisted conductors was also performed in CERN. The application of the developed cables in the LHC is planned in 2024 when all equipment related to the HL-LHC will be mounted. The total amount of the  $MgB_2$  wire required for the serial production of superconducting assemblages is  $\sim 1000$  km [82, 92].

The HL-LHC program has created the European initiative project FP7 BESTPATHS (abbreviation of

Beyond State-of-the-Art Technologies for Power AC Corridors and Multi-Terminal High Voltage Direct Current Systems), according to which, currently, the full-scale power network for 320 kV is developed. The  $MgB_2$  cable system is intended for the transmission of an electric power of 3.2 GW and a current of 10 kA at 20 K. The studied cable has the same geometry (18  $MgB_2$  filaments spirally twisted around a copper core [91]) and the used scheme of wires is similar to that used in the cables developed for the HL-LHC CERN project [92]. This is the joint project realized by 40 leading European countries in the field of science and industry, which is supported by the Seventh Framework Program for Research of the European Commission [93].

In terms of the project, an experimental individual sector of distributive power grid, the so-called DEMO 5, was created. This is the first attempt to use  $MgB_2$  as the superconductor for HVDC cables [94].

Among the possible applications, the potential use for the future tokamak IGNITOR should be noted. The main idea of the project is to reach conditions for the ignition of thermonuclear plasma only with the ohmic heating at the expense of a current passing in the toroidal direction without the involvement of powerful facilities for the additional heating. The IGNITOR is based on copper coils operating at cryogenic temperatures  $\sim 30$  K at the expense of forced gaseous helium flow. The promising aspects of project IGNITOR are the creation of high-volume high-field magnetic systems using a cryoresistive conductor, a unique multifunctional energy complex, a system for the physical and technological diagnostics of dense thermonuclear plasma, and a system for intelligent control of processes occurring in plasma. This project can initiate the application of  $MgB_2$  in thermonuclear fusion technologies [82].

#### *Production Methods of $MgB_2$ Wires*

The following production methods of magnesium diboride-based superconducting wires exist: “powder-in-tube” (PIT) and magnesium diffusion methods; they were considered in the section related to the synthesis methods for the magnesium diboride. The production of  $MgB_2$ -based superconductors by PIT method can be realized by two ways. In the first case, the method is called in situ; in this case, as the initial powder, the magnesium and boron mixture is used, and the superconducting compound forms as a result of the synthesis of finished conductor in a temperature range 600 to 700°C, which corresponds to the so-called low-temperature synthesis. In the case of the ex situ method, the  $MgB_2$  compound is synthesized in advance. For this purpose, the direct synthesis of the magnesium and boron mixture is realized in a temperature range above the melting temperature of magnesium; this is the so-called high-temperature synthe-



sis. After that, the prepared powder is used to produce composite wires, in which the superconducting filaments are formed from the magnesium diboride powder [95]. Both the in situ and ex situ methods have advantages and disadvantages. The low cost and availability of the magnesium and boron mixture and the sufficient simple way of introduction of alloying elements are the advantages of the in situ method; the disadvantage is the prolonged annealing of finished articles for the formation of superconducting phase. The advantages of the ex situ method are the higher density of superconducting core and the absence of the necessity to perform prolonged annealings since the core is filled up with the finished superconductor. The disadvantage is the complicated and labor-consuming method for the production of MgB<sub>2</sub> powder of required composition with the optimum granule sizes.

In [96], a combined in situ and ex situ method was used; in this case, the advantages of each of the methods are realized. In terms of this study, the alloyed magnesium and boron mixture (in situ) and the finished MgB<sub>2</sub> powder (ex situ) were used to produce samples of wire  $(\text{MgB}_2)_x + (\text{Mg} + 1.99\text{B} + 0.01\text{C})_{1-x}$ , where  $x = 0, 0.3, 0.5, 0.7,$  and  $1.0$ . In [96], the effect of the ratio of in situ and ex situ powders on the phase composition, structure, critical temperature ( $T_c$ ), and critical current ( $J_c$ ) of the produced superconductor was studied. The study of the microstructure showed that the amount of Kirkendall pores decreases as  $x$  decreases; therefore, the density of superconducting core increases. One of the factors of the increase in the density is the ability of magnesium from the in situ powder to close cracks and enhance the coupling between the in situ and ex situ areas. The samples with  $x = 0.5$  and  $x = 0$  have the highest and lowest temperature,  $T_c = 38.54$  and  $T_c = 37.26$  K, respectively. The other samples have the intermediate temperatures  $T_c$ . The sample with  $x = 0$  exhibits the highest value of  $J_c$ , whereas the samples with  $x = 0.7-1.0$  have the lowest values of  $J_c$  in magnetic fields of 4–10 T. This is explained by the authors as the effect of alloying and by the presence of cracks. The other samples have the intermediate values of  $J_c$ .

Authors of [97] have suggested the production method of MgB<sub>2</sub>/Cu wire that exhibits improved current characteristics; the double-core method is used. The essence of the method consists in the fact that the in situ core is located inside the conductor, whereas the ex situ core is located from the outside; the wire is covered with a copper shell. Figure 7 shows the cross-section of the wire.

This method allowed the authors to improve the current carrying ability of the conductor as compared to that of the analogous reference in situ wire by 3.5 times and ensures the critical current density  $J_c = 1.2 \times 10^3$  A/cm<sup>2</sup> at 6 T. The authors assume that the main cause for the improvement of the current carry-

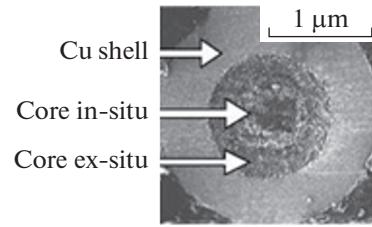


Fig. 7. Cross section of wire with two cores [97].

ing ability is the fact that the outside core prevents the reaction of starting materials of the inside in situ core with the copper shell during heating.

The diffusion method is of interest owing to the fact that it allows one to produce conductors with the higher current carrying ability as compared to that of conductors produced by PIT method. The internal and external diffusion methods exist. The internal diffusion method consists in the following. A magnesium rod is placed in the center of a metallic shell, and a boron powder is filled up around the rod. In the case of external diffusion of magnesium, a boron powder is located in a magnesium tube with the external shell made from, for example, iron or another metal suitable for this purpose. During thermomechanical treatment, magnesium diffuses into the boron layer surrounding magnesium with the formation of the superconducting phase. The authors of [98] have fabricated 7-filamentary conductors by internal magnesium diffusion (IMD). A pure magnesium rod 2 mm in diameter was put into a Ta tube. The space between the magnesium rod and Ta tube was filled up with the mixture of boron powder with 10 wt % SiC. After rolling and drawing, seven cuts of unifilar conductors were combined and put into a tube made from the Cu–10 wt % Ni alloy. After that, the composite comprising seven cores was subjected to cold rolling in passes and to drawing. The total reduction of area of the initial composite to 7-filamentary conductor was ~95%. The 7-filamentary conductor was heated at 640°C for 1 h in an argon atmosphere to crystallize MgB<sub>2</sub>. The authors relate the increase in the critical current of the wire prepared by IMD method, as compared to that of the wire prepared by PIT method, to the microstructure of the wire. The superconducting layer is the dense polycrystalline MgB<sub>2</sub> compound with a grain size of 20–200 nm. Within the layer, fine MgO and Mg<sub>2</sub>Si particles 10–30 nm in size are dispersed. In this case, the outer area near the Ta shell consists of unreacted B and SiC powders, fine MgO particles, and small pores. The pore sizes for the IMD MgB<sub>2</sub> conductor are less than those for the PIT MgB<sub>2</sub> conductor. The oxidation of Mg in the course of IMD process leads to the formation of fine MgO particles, which can be efficient fluxoid pinning centers.

The authors of [99] produced conductors, by IMD method, with the critical current density  $J_c = 1.07 \times$

**Table 1.** Composition (vol %) of MgB<sub>2</sub> wire

Method	Nb	Cu	Ni	Cu–Ni	NbNi <sub>3</sub>	MgB <sub>2</sub>
Ex situ	15	–	17	46	6	16
In situ	30	13	–	38	–	19

10<sup>5</sup> A/cm<sup>2</sup> and engineering critical current density  $J_e = 1.67 \times 10^4$  A/cm<sup>2</sup> at 10 T and 4.2 K. The critical current density, which exceeds the highest values of  $J_c$  previously found for IMG conductors by 3.5 times, was explained by the authors by the correct selection of B powder, fraction density, and growth mechanism of the MgB<sub>2</sub> layer.

### *High-Current MgB<sub>2</sub> Cables*

The production of long composite superconductor is the very complicated and multifarious process. Manufacturers face difficulties in choosing deformation methods, deformation rate, and conditions of intermediate annealings. Wrong decisions in choosing technological treatment conditions can lead to failure of the composite as a whole.

Authors of [100] studied the mechanical properties of MgB<sub>2</sub> wire fabricated by ex situ and in situ method after uniaxial tensile loading at room temperature ( $T_r$ ) and at 77 K and the effect of this loading on the degradation of the critical current. The composition of the wire is given in Table 1.

At 77 K, wires can withstand the higher stresses as compared to those withstood at room temperature. In order to explain what factors affect the degradation of conductors, lattice distortions of various components of wire and their structure after loading were studied in [100]. The microstructure of cross-sections of filaments varies in accordance with the degree of loading. It was shown that Cu and Ni introduce only insignificant contribution to the strength of wire, whereas Cu–Ni alloys and Nb are characterized by some elasticity and increase the mechanical strength of wire. The authors assume that the strength of MgB<sub>2</sub> wires upon drawing can be increased at the expense of armoring with corrosion-resistant steel.

In [101], the correlation between the critical current  $J_c$  and structure of unifilar MgB<sub>2</sub> composites subjected to cold drawing and annealing at 600 and 700°C for 71 h was studied. As the grain size increases with increasing annealing time, the critical current density decreases monotonously and nonlinearly. The magnetic field applied both in perpendicular and longitudinal directions leads to the untimely degradation of conductors, which is related by the authors to the formation of intergrain films and MgO particles at boundaries. This leads to the decrease in the intergrain conductivity. Thus, the destroyed coupling between

MgB<sub>2</sub> grains in the superconducting conductor leads to the increase in the dependence of  $J_c$  on the field.

The thermal stability of a superconducting device is the important quality, whatever the field of application of conductor. In the case of overheating of the conductor, the temperature of the conductor can increase locally to values that exceed the temperature at which the separation of the transport current between the superconductor and metals present in the composite starts. In this case, the heat is generated at the expense of the Joule effect, and the transition of the whole system from the superconducting to normal state can occur. In [102], the study of the thermal transport properties of multifilamentary MgB<sub>2</sub> ribbons differing in the structure and composition of materials are studied. The longitudinal and transverse components of the thermal conductivity were measured and the effect of the field on the heat conductivity was studied. Different constituent materials and types of stabilization of conductors allowed the authors to compare the constructions of MgB<sub>2</sub> ribbons and thermal properties of these wires and, thus, to obtain information on optimizing the thermal stability of superconductor. The stability in the case of local overheatings of ribbons can be improved at the expense of either use of copper with the high residual resistance or increase in the volume specific heat of conductor via the selection of suitable materials for the matrix.

To stabilize the wire at cryogenic temperatures against the thermal surge, a shell component characterized by the high electrical and thermal conductivities is desirable. The selected shell or composite material substantially affect the current carrying ability of MgB<sub>2</sub> wires, which is due to the cold resistance, ability of the shell to react with Mg and B, and compatibility of thermal contraction of conductor and composite. Not all combinations of materials are suitable for the shells. The conducting materials, such as Cu, can act as the parallel shunt for improving the thermal stability. However, the materials such as Cu and Ni are highly reactive for Mg in conductors fabricated by the in situ method; because of this, a barrier is needed in order to avoid the formation of reactive layers between the conductor and shell. Traditional barrier materials, such as Nb and Ta, have disadvantages such as the lower coefficient of thermal expansion as compared to that of MgB<sub>2</sub>. This can lead to microcracks and densification of filament during cooling from the heat-treatment temperature to the operation temperature if the slight compression of barrier material is not compensated by outer shell with the higher compression. The authors of [103] achieved the engineering transport critical current density  $J_e = 55$  kA/cm<sup>2</sup> ( $J_c = 387$  kA/cm<sup>2</sup>) at 4.2 K and 3 T for the MgB<sub>2</sub> wire fabricated by the in situ method with Nb barrier and Cu stabilizer that was armored with corrosion-resistant steel; the wire thickness was only 164 nm. The critical current densities of 7-filamentary MgB<sub>2</sub>/Cu conduc-

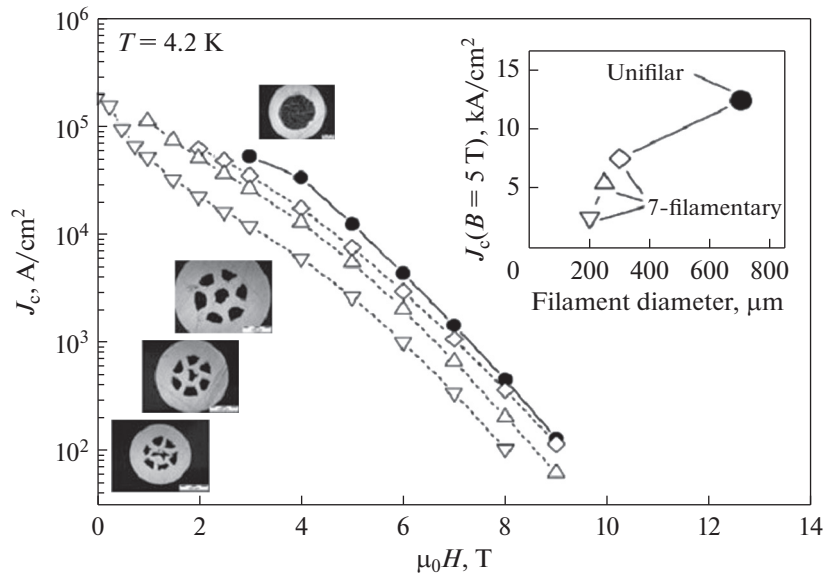


**Fig. 8.** Critical current of 1- and 7-filamentary MgB<sub>2</sub>/Cu conductors with different outer and filament diameters at 4.2 K as a function of the magnetic field. Inset shows the decrease in  $J_c$  at 5 T as the filament diameter decreases [103].

tors of different diameters are lower than  $J_c(B)$  for the unifilar conductor and decreases as the filament diameter decreases. The decrease in  $J_c$  is due to the fact that the Cu shell tends to react with Mg present in the conductor; as the conductor diameter decreases, the fraction of reaction layer in the total volume of conductor becomes higher. Moreover, in the case of additional deformation stages, the geometry of filaments worsens since copper is too soft to hold the filament shape with the powder Mg and B mixture (Fig. 8).

The current input in a superconducting wire is an important problem. In [104], temperature-dependent current carrying properties of superconducting MgB<sub>2</sub> wires with the copper and iron shells were studied via the estimation of the length of current transfer from the matrix into superconducting area through a high-resistance barrier layer in different cross sections and the combination of section areas of superconducting core, barrier, and inside metallic shell. The term “current transfer length” (CTL) is defined in [105]. The lowest CTL ( $\sim 0.2$  mm) was obtained for wires in the Fe shell (MgB<sub>2</sub>)/V/Fe for all studied combinations of the section area over the wide temperature range (10–25 K) as compared to that of wires in the Cu shell (MgB<sub>2</sub>)/V/Cu). The change in the CTL with changing operating temperature is not high for both types of the studied superconducting wires. The calculated values of CTL of the MgB<sub>2</sub>/V/Fe superconducting wires are less than 1 mm for all the studied combinations at all operating temperature. The estimation of the density of heat flow generated in the metallic shell assumes that electric loss is lower for the superconducting wires with the Fe shell. Thus, the result of the study shows

that the MgB<sub>2</sub>/V/Fe combination can be favorable for manufacturing superconducting wires.

It was shown in [106] that additional mechanical deformation of MgB<sub>2</sub> cable before heat treatment leads to the substantial increase in the critical currents at the expense of the improved MgB<sub>2</sub> core density;  $J_c$  (4.2 K, 10 T) and  $J_c$  (20 K, 5 T) =  $1 \times 10^4$  A/cm<sup>2</sup>.

The effect of high-pressure cold deformation and subsequent high-temperature recovery annealing on the grain size of bulk MgB<sub>2</sub> samples is discussed in [64]. Despite the slight increase in the grain size, the annealing of deformed MgB<sub>2</sub> leads to the increase in the critical current density by  $\sim 3$  times as compared to the values observed for the initial state (to  $6.7 \times 10^4$  A/cm<sup>2</sup> at 30 K); this is related by the authors to the healing of cracks as a result of deformation and increasing coupling between MgB<sub>2</sub> phase grains.

The structure of the core of unifilar MgB<sub>2</sub>/Cu,Nb composite with a critical current of 427 A (0 T, 4.2 K;  $J_c > 10^5$  A/cm<sup>2</sup>), which was prepared by the ex situ method, was studied in [107]. Two types of MgB<sub>2</sub> crystals were observed; these are large and very dense crystals with the low oxygen content (2–8 at %) and fraction of small loosely coupled crystallites characterized by the low magnesium and boron contents and high oxygen content (4–21 at %). It was shown that the fraction with loose grains negatively affects the critical current density.

The problem of the firm adherence of MgB<sub>2</sub> grains to each other is discussed in [108]. This study was performed in terms of the modernization of LHC in CERN in order to use MgB<sub>2</sub> wires in high-current

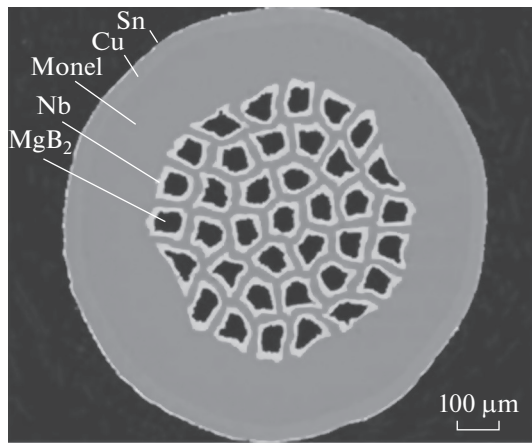


Fig. 9. Cross section of MgB<sub>2</sub> wire [91].

cables. It is known that the mechanical properties of a material used for the fabrication of cable are a key for the determination of the cable construction and manufacturing conditions. The authors estimated the Young modulus of MgB<sub>2</sub> filaments extracted from composite ex situ wires. Two types of round wires were selected. One of the wires comprises 30 MgB<sub>2</sub> filaments each of which is surrounded by niobium barrier in Ni matrix. The copper core is located in the center of wire; Monel (Ni–Cu alloy) is located in the outer layer. This wire was used for manufacturing a cable prototype 10 m long with a current load of 3.5 kA at 27.5 K. The other wire consists of 37 MgB<sub>2</sub> filaments, a Nb barrier around each of the filaments, a Ni matrix, and Monel in the outer layer. The central copper core in the wire is substituted by MgB<sub>2</sub> filament. The Cu stabilizer is added galvanically and does not enter into cross-section. Filaments consisting of MgB<sub>2</sub>, Nb, and Nb–Ni were extracted by chemical etching of the wire; their Young modules, which were determined by tensile tests of single filament, are 114 and 122 GPa, respectively. In assuming that Ni<sub>3</sub>Nb in single filament has an arbitrary orientation, the Young modulus of MgB<sub>2</sub> filaments extracted from wires of two different geometries is 62 and 84 GPa, respectively. These values are substantially lower than the values available for very dense bulk MgB<sub>2</sub>. Based on these results, the authors assume that MgB<sub>2</sub> filaments are substantially porous.

The study [91] is devoted to the investigation of mechanical properties of new-generation round MgB<sub>2</sub> wires. In recent years, cooperative investigations performed by CERN and Columbus Superconductors led to the development of several configurations of MgB<sub>2</sub> wires. This study was aimed at reaching the best superconducting properties for high-current MgB<sub>2</sub> cables for the modernization of LHC in CERN (HL-LHC program). In addition to good electrical characteristics, the superconductor must have the adequate

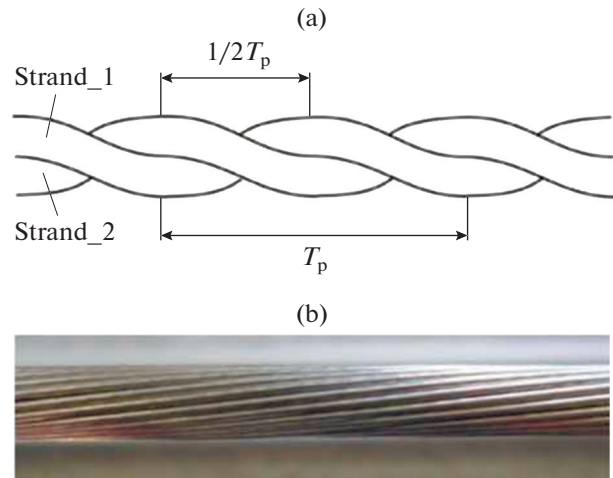


Fig. 10. (a) Schematic image of 2-filamentary cable with indicated twist pitch ( $T_p$ ) and half-twist pitch ( $1/2T_p$ ). (b) Portion of cable 1 m long consisting of Cu core and 18 MgB<sub>2</sub> filaments [91].

mechanical strength with allowance for possible stresses during operation and, in particular, during cabling. Thus, the study of the mechanical properties of MgB<sub>2</sub> wires is critical for designing a cable and its functional use. All results discussed in [91] are assumed to be used for the optimization of 18-filamentary MgB<sub>2</sub> cable configuration in terms of program HL-LHC. The critical current was measured at 4.2 K in a field of 3 T using a wire fabricated by the ex situ method from 37 MgB<sub>2</sub> filaments and subjected to deformation. Figure 9 shows the cross section of the wire. It was found that the decrease in the critical current by 5% takes place at 0.35% deformation. Tensile tests and the estimation of the Young modulus ( $E = 151 \pm 2$  GPa) and yield stress ( $\sigma_y, 0.2\% = 244 \pm 3$  MPa) were performed at room temperature. The critical bending radius and critical pitch strands were determined taking into account the mechanical characteristics of the wire at room temperature and at 4.2 K. The superconducting cable 1 m long consisting of the copper core and 18 MgB<sub>2</sub> filaments was fabricated by twisting (Fig. 10). The wires and extracted conductors were tested at 4.2 K in a field of 3 T. The measurements showed the absence of degradation of the critical current to the twist pitch  $T_p = 170$  mm.

In [90], the fabrication process and critical current characteristics of 30-filamentary superconducting MgB<sub>2</sub> wire and superconducting cables with the (6 + 1) structure, which are based on the wire fabricated by the in situ PIT method, are described. The wire for MgB<sub>2</sub> precursors was prepared by traditional PIT method in Nb tubes. After that, Nb tubes with the Mg and B powders were placed into Cu tubes. The assembled unifilar Cu/Nb/Mg–B composites were rolled and drawn to hexagonal rods 2.65 mm in cross-section

width. Thirty unifilar composite rods and seven Nb—Cu rods of the same size we assembled in a Monel tube. Subsequently, the assembled multifilamentary composite facing was subjected to rolling and drawing with required annealings to a final diameter of 1.0 mm. Six 30-filamentary MgB<sub>2</sub> precursor wires assembled around single copper wire located in the center were twisted to form cables with 3 different twist pitches. Results of metallographic analysis show that the 30-filamentary MgB<sub>2</sub> wire has the adequate homogeneity along both transverse and longitudinal directions, whereas the critical current ( $I_c$ ) and the critical current density ( $J_c$ ) at 4.2 K and 4 T reach 82.6 and  $7.3 \times 10^4$  A/cm<sup>2</sup>, respectively. For the superconducting MgB<sub>2</sub> cable with the (6+1) structure and the twist pitch  $T_p = 50$  mm,  $I_c$  reaches 467 A at 4.2 K and 4 T. After twisting, the existence of eigenfield of tested cable does not decrease  $I_c$  of the MgB<sub>2</sub> wire. This study shows that the MgB<sub>2</sub> superconducting cables are of practical importance.

To sum up the section, it should be noted that MgB<sub>2</sub> still attracts the interest of investigators owing to its fundamental physical properties and practical applications. The leading world companies produced the superconducting wires, such as Columbus Superconductor (Italy), Hypertech (USA), Hitachi (Japan), WST (China), KAT (Korea), currently, fabricate MgB<sub>2</sub>-based wires of different standard sizes by different methods, and new developments for fabricating superconducting MgB<sub>2</sub> wires and cables are performed.

### SUPERCONDUCTING MgB<sub>2</sub> FILMS

The second most promising practical application of magnesium diboride-based materials is superconducting electronics. The basis for the use of superconducting compounds in electronic devices is preparation technologies of thin films and heterostructures based on them, which are deposited on dielectric substrates. The progress in developing MgB<sub>2</sub> thin films results from the success in overcoming a number of serious difficulties that include the volatility of Mg and phase stability of MgB<sub>2</sub>, low sticking coefficients of Mg at high temperatures, and reactivity of Mg for oxygen [109].

Because of the extraordinary chemical reactivity of magnesium, the preparation technologies of MgB<sub>2</sub> thin films are based on the deposition of evaporated components of MgB<sub>2</sub>. These methods include the coevaporation of the components using resistive vapor sources and the evaporation of one of the components with the resistive vapor sources and evaporation of the other component with an electron beam, laser deposition followed by ex situ annealing, molecular-beam epitaxy, magnetron sputtering of targets, and hybrid physical—chemical vapor deposition (HPCVD). Cur-

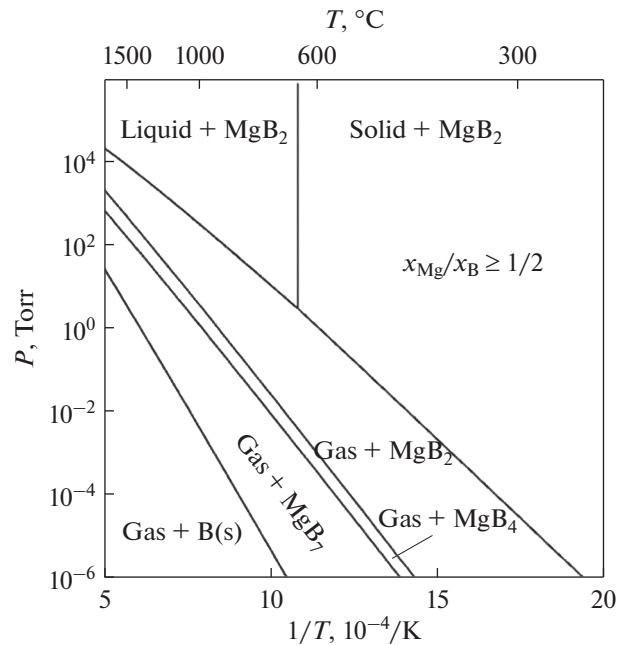


**Fig. 11.** Pressure—temperature phase diagram for the atomic ratio Mg : B  $x_{Mg}/x_B \geq 1/2$ . The composition window marked as Gas + MgB<sub>2</sub> corresponds to the MgB<sub>2</sub> film growth [111].

rently, HPCVD is one the most challenging methods; it allows one also to realize the epitaxial growth [110].

### Deposition of MgB<sub>2</sub> Films

The deposition process of MgB<sub>2</sub> films is difficult owing to the following factors.

Since Mg is volatile and MgB<sub>2</sub> decomposes at high temperatures at the insufficient vapor pressure of Mg, the most important requirement for the deposition of MgB<sub>2</sub> films at high temperatures is to provide the high Mg vapor pressure.

According to the pressure—temperature phase diagram (Fig. 11), the window of corresponding to the growth of MgB<sub>2</sub> films (marked as Gas + MgB<sub>2</sub> region) is in line with the very high Mg vapor pressure that is necessary to ensure the thermodynamic stability of MgB<sub>2</sub>. For example, the deposition at a temperature of 750°C, which is desirable for growing epitaxial thin films, calls for a Mg pressure of more than 44 mTorr (1 mTorr = 0.133322 Pa). A decrease in the deposition temperature leads to the violation of the crystal structure of films. For example, the Mg pressure necessary for the phase stability is  $\sim 10^{-8}$  Torr at 300°C. The deposition of MgB<sub>2</sub> is the process that occurs with the participation of volatile elements; the MgB<sub>2</sub> film composition can be controlled automatically until the Mg partial pressure is within a sufficiently wide growth window, and the Mg : B ratio is more than 1 : 2 [109].

To grow pure  $\text{MgB}_2$  films, it is of high importance to prevent the contamination of them with oxygen and carbon in growing. Magnesium actively reacts with oxygen; it was shown that the deposition of  $\text{MgB}_2$  at 250–300°C and a background pressure (arbitrary pressure of pure nitrogen) of  $3 \times 10^{-8}$  Torr leads to the formation of insulating films. The oxidation of Mg decreases the efficient Mg vapor pressure and results in the formation of MgO that prevents the growth of  $\text{MgB}_2$  grains. This leads to the formation of a nanocrystalline structure [112] and low superconducting properties. The contamination with carbon in the course of the film growth is related to its presence in the starting materials, in particular, in targets used for sputtering or laser ablation and decreases the critical temperature ( $T_c$ ) of  $\text{MgB}_2$ . However, the oxidation [110] and alloying with carbon [113, 114] can favor the increase in the  $\text{MgB}_2$  upper critical field.

#### *Annealing of Films in Mg Vapor*

The first successful method realized for the preparation of high-quality  $\text{MgB}_2$  films is the deposition of film precursors of boron and Mg–B mixture at low temperatures and their annealing in Mg vapor at high temperatures. The film precursors can be prepared by pulsed laser deposition [26], magnetron sputtering [115], electron-beam evaporation [116], thermal evaporation [117], chemical vapor deposition (CVD) [118], and screen printing [119]. The annealing of film precursors often is performed in a hermetical chamber at a temperature of more than 850°C using metallic Mg pieces. This ensures the high Mg vapor pressure that is required for the phase stability at the high temperature of the process.

Thin  $\text{MgB}_2$  films prepared in the course of a two-stage process that includes the deposition and annealing are epitaxial [120]. The superconducting properties of these films are also the best:  $T_c \sim 39$  K [26, 115] and the very high critical current density  $J_c$  that exceeds  $10^7$  A/cm<sup>2</sup> in zero magnetic field [121]. However, often it is difficult to avoid the contamination with oxygen and carbon, which takes place upon deposition of film precursor. Oxygen enters into the films, because of the low background vacuum during deposition, and carbon is present in the starting materials. The use of CVD and hydrogen as the carrier gas and diborane ( $\text{B}_2\text{H}_6$ ) as the boron source allowed one to prepare high-purity boron films [122]. The annealing in Mg vapor is carried out in a pure Ar atmosphere in hermetical carbon-steel tube. The 3  $\mu\text{m}$   $\text{MgB}_2$  film prepared in such a way on a SiC substrate exhibits the abrupt superconducting transition at 40 K, a low residual electrical resistivity of 1.2  $\mu\Omega/\text{cm}$ , and sufficiently high residual resistance ratio (RRR) equal to 10, which indicates the fact that the film is uniform and pure.

A variant of the two-stage annealing is the annealing of film precursor in situ after its deposition in Mg vapor that forms locally from excess Mg present in the film precursor. The film precursors and  $\text{MgB}_2$ , Mg +  $\text{MgB}_2$  or Mg + B multilayers are deposited in a temperature range from room temperature to 300°C by pulsed laser deposition [112, 123], sputtering [124], thermal evaporation [117], and electron-beam evaporation [125]. After that, they are heated in the growth chamber to different annealing temperatures and for different times to form the  $\text{MgB}_2$  phase that does not decompose (the local Mg vapor pressure varies in the course of annealing and, finally, drops). This calls for the careful balance between the processes. The  $\text{MgB}_2$  films prepared in such a way often are nanocrystalline and exhibit a lower  $T_c$  temperature [112, 123].

#### *Physical Deposition from Vapor*

The  $\text{MgB}_2$  superconducting films can be prepared by at-once in situ deposition that was first demonstrated in [126] by pulsed laser deposition at 400–450°C. The deposition of  $\text{MgB}_2$  films at low temperatures allows the authors to avoid the necessity of the high Mg vapor pressure. In order to prevent the contamination with oxygen, an ultrahigh-vacuum background pressure that is more than  $10^{-8}$  Torr is required [127–129]. It is shown that it is of importance to use the pure Mg metal source in order to avoid the contamination with oxygen and carbon. In [128, 129], to deposit the  $\text{MgB}_2$  superconducting films, the molecular beam epitaxy was used; the substrate temperature was in a range from 150 to 320°C. For the film deposited on the substrate at 320°C,  $T_c \sim 36$  K. The authors of [130] showed that the  $\text{MgB}_2$  grain size in such films can reach 400 Å.

To improve the crystal structure, namely, to improve the purity of film and its epitaxial perfection and to reach the optimum grain size, a high deposition temperature is necessary, which calls for the high Mg pressure and decrease in the oxygen contamination. This was shown in [131] via the in situ preparation of thin  $\text{MgB}_2$  films, which combines the Mg evaporation from an intense vapor source and sputtering of B in ultrahigh vacuum; the film deposited at a substrate temperature of 440°C had  $T_c = 33$  K.

The most successful physical vapor deposition method used for growing  $\text{MgB}_2$  films is the reactive chemical evaporation (RCE) that is reported in [132]. The films were grown using a rotary heater. The high quality of the  $\text{MgB}_2$  films deposited at a temperature of 550°C was noted. This technology allows one to grow two-side large-area films in intermediate layers of multilayer films.

### Hybrid Physicochemical Deposition from Vapor

Among all the deposition methods of MgB<sub>2</sub> films, hybrid physicochemical vapor deposition (HPCVD) was found to be most efficient. In terms of this method, Mg vapor is prepared by thermal evaporation of bulk pieces (physical vapor deposition), whereas boron is taken from the B<sub>2</sub>H<sub>6</sub> diborane gas precursor (chemical vapor deposition). This method ensures the high Mg vapor pressure that satisfies the conditions of thermodynamic stability of the phase at the deposition temperature and uses the reducing hydrogen atmosphere during deposition, which suppresses the Mg oxidation. In the case of the original HPCVD system realized at the University of Pennsylvania [133], a graphite heater with the SiC coating was used to heat both a substrate and Mg pieces located near the substrate. During induction heating of the substrate to ~700°C in hydrogen (carrier gas) at a pressure of 100 Torr, bulk Mg pieces also are heated and produce the high Mg vapor pressure near the substrate. When a gas mixture is introduced into the reactor, MgB<sub>2</sub> starts to grow. The deposition stops when the B<sub>2</sub>H<sub>6</sub> gas supply stops, and the film is cooled to room temperature in the hydrogen atmosphere. Figure 12 shows the structure of the film.

The selection of substrates directly affect the quality of thin MgB<sub>2</sub> films. To prepare the MgB<sub>2</sub> film, Al<sub>2</sub>O<sub>3</sub>-R, Al<sub>2</sub>O<sub>3</sub>-C, Si(100), Si(111), SrTiO<sub>3</sub>(100), MgO(100), and SiC(0001) are usually used. Since MgB<sub>2</sub> has the hexagonal structure, materials with the hexagonal structure should be used for substrates [134].

According to data of [135], 4H-SiC and 6H-SiC are ideal substrates for thin MgB<sub>2</sub> films. In zero field,  $J_c$  is  $3.5 \times 10^7$  A/cm<sup>2</sup> at 4.2 K and above  $10^7$  A/cm<sup>2</sup> at 25 K.

High-purity epitaxial MgB<sub>2</sub> films were prepared by HPCVD owing to the reducing H<sub>2</sub> atmosphere and high-purity Mg and B sources used in this technology [133, 136]. The purity of films deposited by HPCVD is higher than that of single crystals [137] and bulk samples. The value of  $T_c$  is higher than that of bulk MgB<sub>2</sub>, because of the deformation-induced phonon softening that increases the electron-phonon interaction [138].

In the original HPCVD system, the Mg partial pressure is related to the substrate temperature; this limits the substrate temperature that is no less than ~700°C, since, as the substrate temperature decreases, the Mg vapor pressure decreases. In modern installations, during deposition of MgB<sub>2</sub> film, it is possible to control the temperature of Mg source and, therefore, the Mg vapor pressure is independent of the substrate temperature.

Modified configurations of HPCVD installations equipped with individual heaters for the Mg source and substrate have been reported. The technique used in [139], when the diborane is supplied in the form of

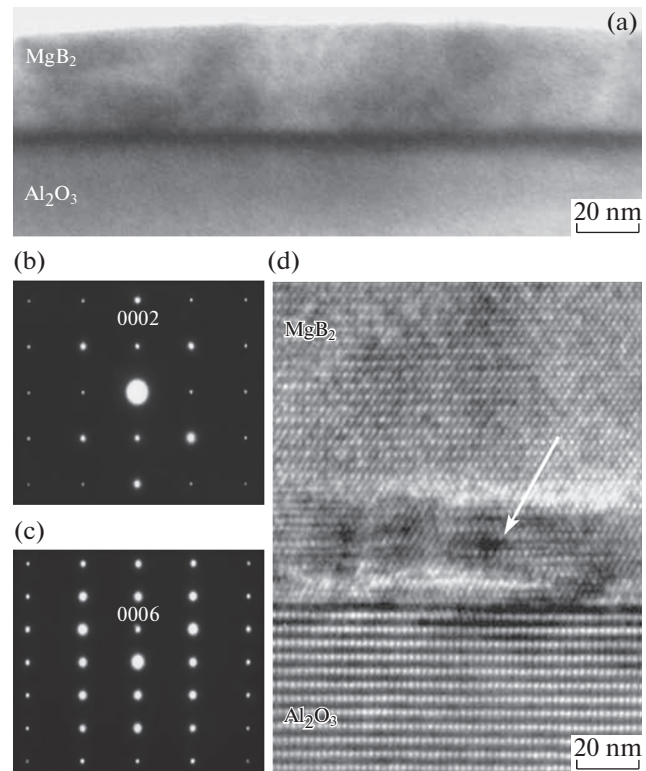


**Fig. 12.** Microstructure and interface atomic structure of cross-section of film studied by TEM: (a) TEM, bright-field image, low magnification; (b) electron diffraction pattern of MgB<sub>2</sub>, zone axis  $[11\bar{2}0]$ ; (c) electron diffraction pattern of sapphire substrate, zone axis  $[10\bar{1}0]$  (direction of incident electron beam corresponds to that in Fig. 12b); (d) high-resolution TEM image of film/substrate interface with an intermediate layer (shown by an arrow) resulted from the overlapped areas of MgO and epitaxially grown MgB<sub>2</sub> [133].

a jet, allowed the authors to deposit MgB<sub>2</sub> films at the very high rate (2μ/min). In [140], the deposition of superconducting MgB<sub>2</sub> films was performed from 350 to 750°C. The film deposited at 620°C has the highest critical temperature  $T_c = 40.8$  K and minimum residual specific resistivity. As the substrate temperature decreases,  $T_c$  decreases, whereas the specific resistivity increases. It was noted that the film deposited at 620°C also has the best crystallinity among the samples. In [141], the pulsed laser deposition of Mg was included in the analogous scheme with the Mg evaporation source, and the MgB<sub>2</sub> films were prepared, which are characterized by  $T_c = 40$  K at ~400°C.

The HPCVD method has demonstrated the efficiency in manufacturing ultrathin films required for the fabrication of superconducting nanowire single-photon detectors (SNSPD). In [142], epitaxial ultrathin MgB<sub>2</sub> films from 6 to 11 nm in thickness were grown on (111) MgO substrates by HPCVD. Their critical temperature  $T_c$  is above 34 K,  $\rho_{4.2K}$  is in a range

of 3–27  $\mu\Omega/\text{cm}$ , and  $J_c = (0.6\text{--}7.7) \times 10^7 \text{ A/cm}^2$  at 2 K, which are comparable with those obtained for ultrathin  $\text{MgB}_2$  films prepared on SiC or  $\text{Al}_2\text{O}_3$  substrates by HPCVD.

#### *Properties of Alloyed $\text{MgB}_2$ Films in High Fields*

The critical current density,  $J_c$ , in a magnetic field is an important parameter for conductors with the high magnetic field. Pure  $\text{MgB}_2$  films demonstrate the high current density in the eigenfield. The value  $J_c = 1.6 \times 10^8 \text{ A/cm}$  at 2 K was obtained in [143] for the film prepared by HPCVD on a bridge 150 nm in width. However,  $J_c$  rapidly suppresses by applied magnetic field, because of the weak pinning in pure films. This is related to the fact that the main pinning mechanism in  $\text{MgB}_2$  is the pinning at grain boundaries, whereas the HPCVD films are characterized by relatively coarse-grained structure with a characteristic grain size of 130 nm [138]. The effect of the grain size also is considered in [144]. The structure of the  $\text{MgB}_2$  films prepared on single-crystal  $\text{Al}_2\text{O}_3$  substrates by ultrasonic pyrolysis was studied after ex situ and in situ heating. The films prepared during in situ heating are characterized by small grain size (less than 50 nm) and, were found to exhibit the much better properties as compared to those of films prepared by ex situ heating, which are characterized by coarse grains (1  $\mu\text{m}$ ). The higher values of  $T_c$  and  $J_c$  are 36 K and  $9.88 \times 10^5 \text{ A/cm}^2$  for the small-grained films, respectively.

The alloying with carbon of  $\text{MgB}_2$  films prepared by HPCVD leads to the substantial improvement of the irreversibility field,  $H_{\text{irr}}$ , and  $J_c(H)$ ; this fact indicates the increase in the flux pinning [145]. The critical current density,  $J_c$ , of the pure  $\text{MgB}_2$  film in the eigenfield is very high and rapidly decreases as an external magnetic field increases. In the case of carbon-alloyed films, despite the fact that  $J_c$  in the eigenfield decreases because of the decrease in both the activation energy of vortices and cross-section area of current conducting layer, the field dependence of  $J_c$  is weaker and  $J_c(H)$  in high fields is substantially higher. Moreover, changes in the microstructure, such as the decrease in the grain size to 5–20 nm and existence of the amorphous intergranular phase [146], favor the increase in the pinning in the carbon-alloyed HPCVD  $\text{MgB}_2$  films. The experimental evidence of the close correlation between the decrease in the grain size and improvement of high-field properties were reported in [143]. The transmission electron-microscopy (TEM) studies showed that the carbon content in  $\text{MgB}_2$  of  $\text{Mg}(\text{B}_{1-x}\text{C}_x)_2$  grains corresponds to  $x < 5\%$  and the fact that the majority of carbon atoms comprises the amorphous intergranular phase. In the films with grain sizes of 5–20 nm, the spacious structural disorder is observed, which includes the lattice rotation with respect to the  $c$  axis and small  $c$ -axis misorientations in neighboring grains. The high electron scatter-

ing resulted from the nanosized disorder can be the cause for the very high  $H_{c2}$  in carbon-alloyed HPCVD films [146]. It is assumed that the specific microstructure of carbon-alloyed HPCVD films is the key for their excellent properties in high magnetic fields as compared to those of bulk carbon-alloyed  $\text{MgB}_2$  and  $\text{MgB}_2$  modified by oxygen alloying and irradiation with particles. It should be noted that the epitaxy and texture is not necessary for reaching the best characteristics in high magnetic fields. The best critical current densities in high magnetic fields were demonstrated for polycrystalline  $\text{MgB}_2$  films prepared by two-stage annealing, which have a grain size of 10–20 nm and are free of epitaxial structure. It is assumed that the increase in  $J_c$  in high fields is related to the decrease in the grain size and small MgO inclusions [109]. For carbon-alloyed films, the alloying substantially increases  $H_{c2}$  that is more than 70 T at a low temperature owing to the unique microstructure consisting of  $\text{MgB}_2$  layers several nanometers in thickness, which are separated by nonsuperconducting  $\text{MgB}_2\text{C}_2$  layers [113].

In [110], the correlation between the structure and superconducting properties of magnesium diboride films prepared by magnetron sputtering and doped with oxygen is discussed.

The density of superconducting critical current of films reaches  $J_c = 1.8 \times 10^7 \text{ A/cm}^2$  in zero magnetic field at 10 K at the expense of Abrikosov vortex pinning at  $\text{MgB}_x\text{O}_r$  particles formed at grain boundaries and within grains.

#### *$\text{MgB}_2$ Heterostructures with Other Materials*

Josephson devices and integrated circuits require the multilayered  $\text{MgB}_2$  compound with the other insulating and metallic materials. After successful deposition of single-layer thin  $\text{MgB}_2$  films, investigations, naturally, became focused on the deposition of multilayered films, in particular,  $\text{MgB}_2/\text{barrier}/\text{MgB}_2$  structures. The structural, chemical, and electrical properties at interfaces are crucial for developing devices and circuits [147].

There is information about obtained transitions, in particular,  $\text{MgB}_2/\text{Al}/\text{Al}_2\text{O}_3/\text{Nb}$  [148],  $\text{NMgB}_2/\text{AlN}/\text{Nb}$  [149],  $\text{MgB}_2/\text{Al}_2\text{O}_3/\text{V}$  [150],  $\text{MgB}_2/\text{barrier}/\text{In}$  and  $\text{MgB}_2/\text{barrier}/\text{Pb}$  [151],  $\text{MgB}_2/\text{MgO}/\text{Au}$ , and  $\text{MgB}_2/\text{Al}_2\text{O}_3/\text{Al}$  [147]. These three-layered transitions are of importance for the demonstration of vitality of various barrier materials and for fundamental research of two-gap superconductivity in  $\text{MgB}_2$ .

Several types of weakly coupled compounds for which only a single  $\text{MgB}_2$  layer is required were studied. Nanobridges are one of the types of the weak coupling [152], which form in  $\text{MgB}_2$  via the nanofabrication. A focused ion beam was used for the preparation



of nanobridges  $\sim 70$  nm in width, 150 nm in height, and 150 nm in length [153], and a SQUID server using these weakly coupled transitions was fabricated, which adequately work at 20 K [109].

In [154], extensive studies of multilayered MgB<sub>2</sub>/Ni and MgB<sub>2</sub>/B films prepared by electron beam evaporation were performed. The critical current density,  $J_c$ , of the multilayered MgB<sub>2</sub>/Ni and MgB<sub>2</sub>/B films in parallel fields was found to be higher than those of single-layer MgB<sub>2</sub> film owing to the introduction of artificial pinning center in the form of nanosized Ni and B layers.

#### *Application of MgB<sub>2</sub> Films*

The MgB<sub>2</sub> compound is of interest for the superconducting electronics mainly owing to the fact that the high  $T_c$  temperature (40 K) of the compound allows one to use Josephson transitions and circuits at a temperature of above 20 K in contrast to Nb-based superconductors that should be cold to 4.2 K. At the same cooling capacity, a cooler for 20 K requires the much lower power consumption, has the much lower weight, and is substantially cheaper, as compared to a cooler for 4 K.

The MgB<sub>2</sub> films can be used in designing RF resonators. A superconducting RF resonator is a key component of accelerators used in the high-energy physics, nuclear physics, synchrotron irradiation sources based on storage rings and free-electron lasers. For example, in new-generation particle accelerators, i.e., in the international linear collider (ILC), 16000 superconducting RF resonators made from pure Nb will be used. Niobium is the material currently used for designing superconducting RF resonators, which exhibits impressive characteristics close to the theoretical limit. The maximum accelerating field for Nb, which corresponds to the surface magnetic field, reaches the values of a critical RF field of 50 MV/m. The further improvement of the characteristics of RF resonators calls for superconductors with the higher critical temperature ( $T_c$ ), higher critical RF field, and higher thermal conductivity; an advantage by the decrease in the cost of cryogenic technique also should take place [109].

An advantage of the use of superconducting thin-film coating of RF cavities also exists [155]. Since the RF field attenuates exponentially from the superconductor surface, the properties of the cavity are determined only by the thin superconducting layer on the cavity surface, whereas the rest of wall serves only as the mechanical support. When a great number of cavities are required, the cost of high-purity niobium can be very high; this fact makes cavities with the thin-film MgB<sub>2</sub> coating highly attractive. Moreover, the use of a material, such as Cu, with the high thermal conductivity for the cavity body can ensure the better thermal stability.

The great potential of using MgB<sub>2</sub> in superconducting RF resonators was recognized by investigators working in this field [156]. Some results showed the potentially high ability of the MgB<sub>2</sub> films, which were prepared by pulsed laser deposition and reactive selective evaporation HPCVD [157], to withstand the high power as compared to the power withstood by Nb films. The study of MgB<sub>2</sub> films for RF resonators has only started. It is necessary to do much work in order to completely understand the potential of these films for this important application [109].

In [158], it was reported about the possibility to form ultrathin film 4.2 nm thick, which exhibits good superconducting properties at a critical temperature of 8 K, a specific resistivity of 1200  $\mu\Omega/\text{cm}$  at 40 K, and an average roughness of 0.18 nm. Such an ultrathin MgB<sub>2</sub> film was epitaxially grown on the Al<sub>2</sub>O<sub>3</sub> substrate by HPCVD method [159]. It has  $T_c = 34$  K (0 T), a specific resistivity of 7.90  $\mu\Omega/\text{cm}$  at 42 K, and a critical current density of  $10^6$  A/cm<sup>2</sup> at 16 K. According to data of [160], the authors have been able to produce hot electron detectors, which showed the high current density equal to  $7.7 \times 10^6$  A/cm<sup>2</sup> at 4.2 K in the 400-nm bridge with a MgB<sub>2</sub> layer 30 nm thick and detectors with the meander line 250 nm in width, 10 nm in thickness, and a critical temperature of 12 K. Thus, the MgB<sub>2</sub> films have the capability to manufacture sensor by lithography for various detectors, such as electron bolometers, superconducting single-photon detectors, and heterodyne mixers.

In [160], the preparation of ultrathin MgB<sub>2</sub> films on sapphire substrates and on the use of them in manufacturing (by lithography) superconducting single-photon detectors (SSPD) and heterodyne mixers with the low noise level and high intermediate frequency are reported. In [159], a method for the fabrication of superconducting nanowires 320–650 nm in width and 1 or 10  $\mu\text{m}$  in length from ultrathin HPCVD MgB<sub>2</sub> films 10 nm thick was suggested. The nanowires with  $T_c$  more than 34 K and  $J_c$  more than  $5 \times 10^7$  A/cm<sup>2</sup> at 20 K can be used for the fabrication of nanodevices such as hot-electron bolometers (HEB) and SSPD with high operating temperatures.

According to the data of [159], 4H–SiC and 6H–SiC are ideal substrates for thin MgB<sub>2</sub> films. In zero field,  $J_c$  is  $3.5 \times 10^7$  A/cm<sup>2</sup> at 4.2 K and is more than  $10^7$  A/cm<sup>2</sup> at 25 K.

There are known attempts to use the MgB<sub>2</sub> films in spintronics for manufacturing current contacts for sensors based on tunnel magnetic transitions [160].

Pure epitaxial MgB<sub>2</sub> films and the films with well-controlled disorder will continue to be of importance for the fundamental studies of two-band superconductivity in MgB<sub>2</sub>. In particular, the study of the MgB<sub>2</sub> films for understanding new effects in physics related

to two-band superconductivity will be significant progress in exploring condensed-matter physics.

In the field of applications of high fields, the study of causes for the substantially higher upper field,  $H_{c2}$ , for the carbon-alloyed HPCVD films as compared to that of bulk samples, remains a focus of research. The development of a conductor with the  $MgB_2$  coating and its tests under laboratory conditions are looming. The recent breakthrough in the field of Josephson tunnel transitions in  $MgB_2/MgO/MgB_2$  opens a new period in the use of them in multilayered schemes, for example, in throwable switch schemes and also for increasing the operation speed and decreasing noise as compared to those of currently available schemes [161].

## CONCLUSIONS

This review summarizes data on the crystal structure of magnesium diboride, its synthesis methods, and the effect of alloying on the critical current density.  $MgB_2$  raised considerable attention as the superconductor for magnets in high magnetic fields. The upper critical field,  $H_{c2}$ , of pure  $MgB_2$  is low, and  $J_c$  is rapidly suppressed by an external magnetic field, because of the absence of pinning centers. The alloying substantially increases  $H_{c2}$  owing to increasing the amount of vortex pinning centers at the expense of grain refining and formation of small particles based on alloying elements, which also can serve as additional pinning centers. Moreover, the review considers the effect of various alloying additions on the critical current density.

Substantial progress in the production technologies of  $MgB_2$  wires with the improved electrical characteristics is noted. Production methods of  $MgB_2$  wires and cables and their potential for further use are described. The first practical use of conductors based on the  $MgB_2$  ribbon is the MRT systems operating around the world. The prospect of using the  $MgB_2$  conductors for the long-distance transfer of high-energy fluxes by "hybrid" hydrogen energy mains is shown.

Currently, the superconducting high-current mains developed in CERN for supplying superconducting magnets of High Luminosity Large Hadron Collider are the most attractive applied project for the  $MgB_2$  superconductor in the world. Project FP7 BESTPATHS deserves special attention; according to the project, the full-scale high-energy transmission system is developed. Among future applications, the potential use of  $MgB_2$  for IGNITOR tokamak is noted. The significant progress of  $MgB_2$  in these directions can lead to the substitution for Nb–Ti conductors.

Various methods used for the fabrication of  $MgB_2$  films are considered in this review. They includes the

annealing of B and Mg–B film precursors in the Mg vapor both ex situ and in situ, physical vapor deposition, and hybrid physicochemical vapor deposition. To deposit the more pure epitaxial  $MgB_2$  films, the HPCVD method is the most successful, since it efficiently meets all key requirements. The brief consideration of depositions conditions was carried out; the conditions include the sufficiently high Mg vapor pressure that ensures the thermodynamic stability of the  $MgB_2$  phase at the deposition temperatures, oxygen-free atmosphere, and pure magnesium and boron sources.

In the field of applications in high fields, the study of causes for the substantially higher upper critical field ( $H_{c2}$ ) of the carbon-alloyed HPCVD films, as compared to that of bulk samples, remains the focus of investigations. The development and testing of a conductor with the  $MgB_2$  coating have top priority. Pure  $MgB_2$  epitaxial films and films with adequately controlled disorder as before will be the matter of fundamental research in the condensed-matter physics. Recent findings in the field of Josephson tunnel transitions in  $MgB_2/MgO/MgB_2$  open the possibility to work on the application of them in multilayered schemes, in particular, in reversible switches.

For summary, we would like to cite the authors of [162], who said that " $MgB_2$  is the excellent present of the nature for the condensed-matter physics."

## FUNDING

This study was performed in terms of the state assignment of the Ministry of Science and Higher Education of the Russian Federation (theme Davlenie, no AAAA-A18-118020190104-3).

## REFERENCES

1. J. Nagamatsu, N. Nakagawa, T. Muranaka, Y. Zenitani, and J. Akimitsu, "Superconductivity at 39 K in magnesium diboride," *Nature* 2001 **410**, 63–64.
2. P. C. Canfield and G. Crabtree, "Magnesium diboride: better late than never," *Phys. Today* **56**, 34–40 (2003).
3. R. J. Cava, "Genie in a bottle," *Nature* **410**, 23–24 (2001).
4. C. Day, "New conventional superconductor found with a surprisingly high  $T_c$ ," *Phys. Today* **54**, No. 4, 17–18 (2001).
5. C. Buzea and T. Yamashita, "Review of the superconducting properties of  $MgB_2$ ," *Supercond. Sci. Technol.* **14**, No. 11, 115–146 (2001).
6. S. L. Bud'ko, G. Lapertot, C. Petrovic, C. E. Cunningham, N. Anderson, and P. C. Canfield, "Boron isotope effect in superconducting  $MgB_2$ ," *Phys. Rev. Lett.* **86**, No. 9, 1877–1880 (2001).
7. D. K. Finnemore, J. E. Ostenson, S. L. Bud'ko, G. Lapertot, and P. C. Canfield, "Thermodynamic and transport properties of superconducting

- Mg<sup>10</sup>B<sub>2</sub>,” *Phys. Rev. Lett.* **86**, No. 11, 2420–2422 (2001).
8. J. M. An and W. E. Pickett, “Superconductivity of MgB<sub>2</sub>: covalent bonds driven metallic,” *Phys. Rev. Lett.* **86**, No. 19, 4366–4369 (2001).
  9. J. Kortus, I. I. Mazin, K. D. Belashchenko, V. P. Antropov, and L. L. Boyer, “Superconductivity of metallic boron in MgB<sub>2</sub>,” *Phys. Rev. Lett.* **86**, No. 20, 4656–4659 (2001).
  10. D. C. Larbalestier, L. D. Cooley, M. O. Rikel, A. A. Polyanskii, J. Jiang, S. Patnaik, X. Y. Cai, D. M. Feldmann, A. Gurevich, A. A. Squitieri, M. T. Naus, C. B. Eom, E. E. Hellstrom, R. J. Cava, K. A. Regan, N. Rogado, M. A. Hayward, T. He, J. S. Slusky, P. Khalifah, K. Inumaru, and M. Haas, “Strongly linked current flow in polycrystalline forms of the superconductor MgB<sub>2</sub>,” *Nature* **410**, 186–189 (2001).
  11. Y. Bugoslavsky, G. K. Perkins, X. Qi, L. F. Cohen, and A. D. Caplin, “Vortex dynamics in superconducting MgB<sub>2</sub> and prospects for applications,” *Nature* **410**, 563–565 (2001).
  12. J. S. Slusky, N. Rogado, K. A. Regan, M. A. Hayward, P. Khalifah, T. He, K. Inumaru, S. M. Loureiro, M. K. Haas, H. W. Zandbergen, and R. J. Cava, “Loss of superconductivity with the addition of Al to MgB<sub>2</sub> and a structural transition in Mg<sub>1-x</sub>Al<sub>x</sub>B<sub>2</sub>,” *Nature* **410**, 343–345 (2001).
  13. M. N. Monteverde, M. Munez-Regueiro, N. Rogado, K. A. Regan, M. A. Hayward, T. He, S. M. Loureiro, and R. J. Cava, “Pressure dependence of the superconducting transition temperature of magnesium diboride,” *Science* **292**, 75–77 (2001).
  14. X. X. Xi, “Two-band superconductor magnesium diboride,” *Rep. Prog. Phys.* **71**, 116501(26) (2008).
  15. T. Takahashi, T. Sato, S. Souma, T. Muranaka, and J. Akimitsu, “High-resolution photoemission study of MgB<sub>2</sub>,” *Phys. Rev. Lett.* **86**, No. 21, 4915–4918 (2001).
  16. G. Karapetrov, M. Iavarone, W. K. Kwok, G. W. Crabtree, and D. G. Hinks, “Scanning tunneling spectroscopy in MgB<sub>2</sub>,” *Phys. Rev. Lett.* **86**, No. 19, 4374–4377 (2001).
  17. R. Osborn, E. A. Goremychkin, A. I. Kolesnikov, and D. G. Hinks, “Phonon density of states in MgB<sub>2</sub>,” *Phys. Rev. Lett.* **87**, No. 1, 017005(4) (2001).
  18. H. J. Choi, D. Roundy, H. Sun, M. L. Cohen, and S. G. Louie, “The origin of the anomalous superconducting properties of MgB<sub>2</sub>,” *Nature* **418**, 758–760 (2002).
  19. W. Pickett, “Mind the double gap,” *Nature* **418**, 733–734 (2002).
  20. I. I. Mazin, O. K. Andersen, O. Jepsen, O. V. Dolgov, J. Kortus, A. A. Golubov, A. B. Kuz’menko, and D. van der Marel, “Superconductivity in MgB<sub>2</sub>: clean or dirty?,” *Phys. Rev. Lett.* **89**, No. 10, 107002(4) (2002).
  21. Y. X. Wang, T. Plackowski, and A. Junod, “Specific heat in the superconducting and normal state (2–300 K, 0–16 T), and magnetic susceptibility of the 38K superconductor MgB<sub>2</sub>: evidence for a multicomponent gap,” *Phys. C* **355**, 179–193 (2001).
  22. F. Bouquet, R. A. Fisher, N. E. Phillips, D. G. Hinks, and J. D. Jorgensen, “Specific heat of Mg<sup>11</sup>B<sub>2</sub>: evidence for a second energy gap,” *Phys. Rev. Lett.* **87**, No. 4, 047001(4) (2001).
  23. P. Szabo, P. Samuely, J. Kacmarcik, J. T. K. Marcus, D. Fruchart, S. Miraglia, C. Marcenat, and A. G. M. Jansen, “Evidence for two superconducting energy gaps in MgB<sub>2</sub> by point-contact spectroscopy,” *Phys. Rev. Lett.* **87**, No. 13, 137005 (4) (2001).
  24. S. Tsuda, T. Yokoya, T. Kiss, Y. Takano, K. Togano, H. Kito, H. Ihara, and S. Shin, “Evidence for a multiple superconducting gap in MgB<sub>2</sub> from high-resolution photoemission spectroscopy,” *Phys. Rev. Lett.* **87**, No. 17, 177006 (4) (2001).
  25. F. Giubileo, D. Roditchev, W. Sacks, R. Lamy, D. X. Thanh, J. Klein, S. Miraglia, D. Fruchart, J. Marcus, and P. Monod, “Two-gap state density in MgB<sub>2</sub>: a true bulk property or a proximity effect?,” *Phys. Rev. Lett.* **87**, No. 17, 177008 (4) (2001).
  26. W. N. Kang, H. J. Kim, E. M. Choi, C. U. Jung, and S. I. Lee, “Superconducting MgB<sub>2</sub> thin films with a transition temperature of 39 K,” *Science* **292**, 1521–1523 (2001).
  27. M. Iavarone, G. Karapetrov, A. Menzel, V. Komaricki, H. You, W. K. Kwok, P. Orgiani, V. Ferrando, and X. X. Xi, “Characterization of off-axis MgB<sub>2</sub> epitaxial thin films for planar junctions,” *Appl. Phys. Lett.* **87**, 242506 (3) (2005).
  28. A. Gurevich and V. Vinokur, “Interband phase modes and nonequilibrium soliton structures in two-gap superconductors,” *Phys. Rev. Lett.* **90**, No. 4, 047004 (4) (2003).
  29. Ya. G. Ponomarev, S. A. Kuzmichev, M. G. Mikheev, M. V. Sudakova, S. N. Tchesnokov, N. Z. Timergaleev, A. V. Yarigin, E. G. Maksimov, S. I. Krasnosvobodtsev, A. V. Varlashkin, M. A. Hein, G. Muller, H. Piel, L. G. Sevastyanova, O. V. Kravchenko, K. P. Burdina, and B. M. Bulychiev, “Evidence for a two-band behavior of MgB<sub>2</sub> from point-contact and tunneling spectroscopy,” *Solid State Commun.* **129**, 85–89 (2004).
  30. D. F. Agterberg, E. Demler, and B. Janko, “Josephson effects between multigap and single-gap superconductors,” *Phys. Rev.* **66**, 214507(5) (2002).
  31. A. Anishchanka, A. F. Volkov, and K. B. Efetov, “Collective modes in two-band superconductors in the dirty limit,” *Phys. Rev.* **76**, 104504 (9) (2007).
  32. H. Suhl, B. T. Matthias, and L. R. Walker, “Bardeen–Cooper–Schrieffer theory of superconductivity in the case of overlapping bands,” *Phys. Rev. Lett.* **3**, 552–554 (1959).
  33. M. Rafieezad, Ö. Balcı, S. Acar, and M. Somer, “Review on magnesium diboride (MgB<sub>2</sub>) as excellent superconductor: Effects of the production techniques on the superconducting properties,” *Boron* **2**, No. 2, 87–96 (2017).
  34. J. Akimitsu, S. Akutagawa, K. Kawashima, and T. Muranaka, “Superconductivity in MgB<sub>2</sub> and Its Related Materials,” *Prog. Theor. Phys. Supp.* **159**, 326–337 (2005).
  35. M. Ranot, P. V. Duong, A. Bhardwaj, and W. N. Kang, “A review on the understanding and fabrication ad-

- vancement of  $\text{MgB}_2$  thin and thick films by HPCVD,” *Prog. Supercond. Cryog.* **17**, No. 2, 1–17 (2015).
36. A. Shikov, “Russian superconductors,” *Natsional'naya Metallurgiya*, No. 2, 83–91 (2004).
  37. R. Kayikci, O. Kurtulus, and R. Gurbuz, “The formation and growth behavior of aluminum boride crystals in an Al–B alloy,” *Solid State Phenom.* **144**, 140–144 (2009).
  38. X. X. Xi, X. H. Zeng, A. Soukiassian, and J. Jones, “Thermodynamics and thin film deposition of  $\text{MgB}_2$  superconductors,” *Supercond. Sci. Technol.* **15**, 451–457 (2002).
  39. A. L. Ivanovskii, “Band structure and properties of superconducting  $\text{MgB}_2$  and related compounds (a review),” *Phys. Solid State* **45**, No. 10, 1829–1859 (2003).
  40. A. L. Ivanovskii, I. R. Shein, and N. I. Medvedeva, “Non-stoichiometric *s*-, *p*-, and *d*-metal diborides: synthesis, properties and simulation,” *Russ. Chem. Rev.* **77**, 467–486 (2008).
  41. Q. Feng, C. Chen, J. Xu, L. Kong, X. Chen, Y. Wang, and Z. Gao, “Study on the formation of  $\text{MgB}_2$  phase,” *Phys. C* **411**, 41–46 (2004).
  42. G. Bovone, D. Matera, C. Bernini, E. Bellingeri, A. S. Siri, A. Malagoli, and M. Vignolo, “Synthesis temperature effects on ex-situ manufactured  $\text{MgB}_2$  wires useful for power applications,” *J. Alloys Compd.* **660**, 342–346 (2016).
  43. E. I. Kuznetsova, S. V. Sudareva, T. P. Krinitsina, Yu. V. Blinova, E. P. Romanov, Yu. N. Akshentsev, M. V. Degtyarev, M. A. Tikhonovskii, and I. F. Kisljak, “Mechanism of the formation and specific features of the structure of massive samples of compound  $\text{MgB}_2$ ,” *Phys. Met. Metallogr.* **115**, 175–185 (2014).
  44. E. I. Kuznetsova, Yu. N. Akshentsev, V. O. Esin, S. V. Sudareva, Yu. V. Blinova, M. V. Degtyarev, V. I. Novozhonov, and E. P. Romanov, “Mechanisms of the formation of a bulk superconducting phase  $\text{MgB}_2$  at high temperatures,” *Phys. Solid State* **57**, 873–879 (2015).
  45. Z. Q. Ma and Y. C. Liu, “Low-temperature synthesis of  $\text{MgB}_2$  superconductors,” *Int. Mater. Rev.* **56**, Nos. 5–6, 267–286 (2011).
  46. J. Ishiwata, M. Muralidhar, N. Koshizuka, K. Inoue, and M. Murakami, “Effect of sintering time on the optimal synthesis condition in  $\text{MgB}_2$ ,” *Phys. Proc.* **58**, 102–105 (2014).
  47. G. Giunchi, “High density  $\text{MgB}_2$  obtained by reactive liquid Mg infiltration,” *Int. J. Mod. Phys. B* **17**, No. 1, 453–460 (2003).
  48. G. Giunchi, “The superconducting properties of high density bulk  $\text{MgB}_2$  obtained by reactive liquid Mg infiltration,” *AIP Conf. Proc.* **824**, No. 1, 813–819 (2006).
  49. A. G. Bhagurkar, A. Yamamoto, BabuN. Hari, J. H. Durrell, A. R. Dennis, and D. A. Cardwell, “Synthesis of dense bulk  $\text{MgB}_2$  by an infiltration and growth process,” *Supercond. Sci. Technol.* **28**, No. 1, 015012 (2015).
  50. T. A. Prikhna, “Modern superconductive materials for electrical machines and devices working on the principle of levitation,” *Fiz. Nizk. Temp.* **32**, No. 4–5, 661–676 (2006).
  51. T. A. Prikhna, W. Gawalek, Ya. M. Savchuk, T. Habisreuther, M. Wendt, N. V. Sergienko, V. E. Moshchil, P. Nagorny, Ch. Schmidt, J. Dellith, U. Dittrich, D. Litzkendorf, V. S. Melnikov, and V. B. Sverdun, “The inclusions of Mg–B ( $\text{MgB}_{12}$ ?) as potential pinning centres in high-pressure–high-temperature-synthesized or sintered magnesium diboride,” *Supercond. Sci. Technol.* **20**, No. 9, 257–263 (2007).
  52. T. A. Prikhna, W. Gawalek, Ya. M. Savchuk, V. M. Tkach, N. I. Danilenko, M. Wendt, J. Dellith, H. Weber, M. Eisterer, V. E. Moshchil, N. V. Sergienko, A. V. Kozyrev, P. A. Nagorny, A. P. Shapovalov, V. S. Melnikov, S. N. Dub, D. Litzkendorf, T. Habisreuther, Ch. Schmidt, A. Mamalis, V. Sokolovsky, V. B. Sverdun, F. Karau, and A. V. Starostina, “Higher borides and oxygen-enriched Mg–B–O inclusions as possible pinning centers in nanostructural magnesium diboride and the influence of additives on their formation,” *Phys. C* **470**, 935–938 (2010).
  53. A. Yu. Potanin, E. A. Levashov, and D. Yu. Kovalev, “Dynamics of phase formation during the synthesis of magnesium diboride from elements in the thermal explosion mode,” *Izv. Vuzov. Poroshkovaya Metallurgiya I Funktsional'nye Pokrytiya*, No. 3, 2–22 (2016).
  54. D. Yu. Kovalev, A. Yu. Potanin, E. A. Levashov, and N. F. Shkodich, “Phase formation dynamics upon thermal explosion synthesis of magnesium diboride,” *Ceram. Int.* **42**, No. 2, 2951–2959 (2016).
  55. C. Xiujuan, X. Tiandong, W. Mingjing, Z. Wenjun, and L. Tianzuo, “Microstructural transformation during combustion synthesis of  $\text{MgB}_2$  superconductor,” *Phys. C* **454**, Iss. 1–2, 38–42 (2007).
  56. S. Zhou, A. V. Pan, J. Horvat, M. J. Qin, and H. K. Liu, “Effects of precursor powders and sintering processes on the superconducting properties of  $\text{MgB}_2$ ,” *Supercond. Sci. Technol.* **17**, 528–532 (2004).
  57. O. I. Lomovsky, G. V. Golubkova, L. S. Dovlitova, V. I. Zaikovskii, and V. I. Maly, “Mechanochemical synthesis of amorphous and crystalline magnesium diboride,” *Inorg. Mater.* **46**, 22–27 (2010).
  58. K. Przybylski, J. Chmista, R. Zalecki, and A. Kolodziejczyk, “Effect of microstructure on properties of  $\text{MgB}_2$  synthesized by SHS method,” *Phys. C* **408–410**, 117–119 (2004).
  59. J. Zhu, Y. B. Zhang, X. L. Niu, C. C. Lu, H. M. Zhu, and C. B. Cai, “Improvement of current-carrying capacity and in situ control of the superconducting fraction of  $\text{MgB}_2$ –MgO composites,” *J. Supercond. Nov. Magn.* **27**, 2205–2209 (2014).
  60. A. V. Kozyrev, T. A. Prikhna, P. P. Barvitskii, A. V. Shaternik, and V. E. Shaternik, “Higher borides and oxygen-containing inclusions as possible pinning centers in superconducting materials based on  $\text{MgB}_2$ ,” *Metallophys. Adv. Technol.* **41**, No. 7, 863–871 (2019).
  61. J. H. Durrell, C. E. J. Dancer, A. Dennis, Y. Shi, Z. Xu, A. M. Campbell, N. H. Babu, R. I. Todd, C. R. M. Grovenor, and D. A. Cardwell, “A trapped field of >3 T in bulk  $\text{MgB}_2$  fabricated by uniaxial hot pressing,” *Supercond. Sci. Technol.* **25**, 112002 (2012).

62. M. Kulich, R. L. Flukiger, C. Senatore, M. Tropeano, and R. Piccardo, "Effect of cold high pressure deformation on the properties of ex situ MgB<sub>2</sub> wires," *Supercond. Sci. Technol.* **26**, 105019 (2013).
63. M. V. Degtyarev, V. P. Pilyugin, Yu. N. Akshentsev, E. I. Kuznetsova, T. P. Krinitsina, Yu. V. Blinova, S. V. Sudareva, and E. P. Romanov, "Influence of high-pressure deformation and annealing on the structure and properties of a bulk MgB<sub>2</sub>," *Phys. Met. Metallogr.* **117**, No. 8, 772–782 (2016).
64. E. I. Kuznetsova, T. P. Krinitsina, Yu. V. Blinova, M. V. Degtyarev, and S. V. Sudareva, "Fine structure of a bulk MgB<sub>2</sub> superconductor after deformation and heat treatment," *Phys. Met. Metallogr.* **118**, No. 4, 364–371 (2017).
65. E. I. Kuznetsova, T. P. Krinitsina, S. V. Sudareva, Yu. V. Blinova, M. V. Degtyarev, and Yu. N. Akshentsev, "Mechanisms of cold deformation under high pressure of superconductive MgB<sub>2</sub> ceramics," *Phys. Met. Metallogr.* **119**, No. 8, 802–209 (2018).
66. D. N. Rakov, A. E. Vorobieva, P. V. Kononov, E. V. Kotova, Yu. N. Belotelova, and M. V. Polikarpova, "Influence of carbon doping on MgB<sub>2</sub> superconducting properties," *Phys. Proc.* **36**, 1480–1485 (2018).
67. X. Zhang, D. Wang, Z. Gao, L. Wang, Y. Ma, Z. Qi, and K. Watanabe, "The doping effect of activated carbon on the superconducting properties of MgB<sub>2</sub> tapes," *Supercond. Sci. Technol.* **21**, No. 7, 075008 (2008).
68. Dadiel J. Longji, M. Muralidhar, and M. Murakami, "Improved superconducting performance of Ag-added nano-diamond doped MgB<sub>2</sub>," *Supercond. Particle Accelerators*, 1105401 (2018).
69. J. Dyson, D. Rinaldi, G. Barucca, G. Albertini, S. Sprio, and A. Tampieri, "Flux Pinning in Y- and Ag-Doped MgB<sub>2</sub>," *Adv. Mater. Phys. Chem.* **5**, No. 10, 426–438 (2015).
70. N. Horhager, M. Eisterer, H. W. Weber, T. Prikhna, T. Tajima, and V. F. Nesterenko, "Ti and Zr doped MgB<sub>2</sub> bulk superconductors," 7th European Conference on Applied Superconductivity, *J. Phys.: Conf. Ser.* **43**, 500–504 (2006).
71. A. G. Bhagurkar, A. Yamamoto, L. Wang, M. Xia, A. R. Dennis, J. H. Durrell, T. A. Aljohani, N. H. Babu, and D. A. Cardwell, "High trapped fields in C-doped MgB<sub>2</sub> bulk superconductors fabricated by infiltration and growth process," *Sci Rep.* **8**, 13320 (2018).
72. J. H. Kim and S. Choi, "Carbon doping induced imperfections on MgB<sub>2</sub> superconducting wire," *J. Anal. Sci. Technol.* **6**, 11 (2015).  
<https://doi.org/10.1186/s40543-015-0048-3>
73. Y. Zhao, Y. Feng, D. X. Huang, T. Machi, C. Hheng, K. Nakao, N. Chikumoto, Y. Fudamoto, N. Koshizuka, and M. Murakami, "Doping effect of Zr and Ti on the critical current density of MgB<sub>2</sub> bulk superconductors prepared under ambient pressure," *Phys. C* **378–381**, 122–126 (2002).
74. D. Goto, T. Machi, Y. Zhao, N. Koshizuka, M. Murakami, and S. Arai, "Improvement of critical current density in MgB<sub>2</sub> by Ti, Zr and Hf doping," *Phys. C* **392–396**, 272–275 (2003).
75. C. Cheng and Y. Zhao, "Enhancement of critical current density of MgB<sub>2</sub> by doping Ho<sub>2</sub>O<sub>3</sub>," *Appl. Phys. Lett.* **89**, 252501 (2006).
76. X. F. Pan, C. H. Cheng, and Y. Zhao, "Effect of rare-earth oxides doping on the superconductivity and flux pinning of MgB<sub>2</sub> superconductor," *J. Supercond. Nov. Magn.* **24**, 1611–1616 (2011).
77. Das S. Sudesh, C. Bernhard, and G. D. Varma, "Enhanced superconducting properties of rare-earth oxides and graphene oxide added MgB<sub>2</sub>," *Phys. C* **505**, 32–38 (2014).
78. W. Li, J. Kang, S. Fu, Y. Hu, P. Hu, M. Zhu, and Y. Li, "Rare earth doping effects on superconducting properties of MgB<sub>2</sub>: A review," *J. Rare Earths* **37**, 124–133 (2019).
79. J. Karpinski, S. M. Kazakov, J. Jun, N. D. Zhigadlo, M. Angst, R. Puzniak, and A. Wisniewski, "MgB<sub>2</sub> and Mg<sub>1-x</sub>Al<sub>x</sub>B<sub>2</sub> single crystals: high-pressure growth and physical properties," *Phys. C* **81**, 408–410 (2004).
80. N. Magnusson, J. C. Eliassen, and A. B. Abrahamsen, SM. Helles, M. Runde, A. Nysveen, L.-E. Moslatt, J. Bjerkli, and P. King, "Fabrication of a scaled MgB<sub>2</sub> racetrack demonstrator pole for a 10-MW direct-drive wind turbine generator," *IEEE Trans. Appl. Supercond.* **28**, No. 4, 5207105 (2018).
81. I. Abdyukhanov, M. Potapenko, M. Alekseev, Yu. Karasev, V. Drobyshev, A. Tsapleva, and E. Dergunova, "Innovative nanotechnology for the production of modern technical superconductors," *Nano industry* **7**, No. 61, 62–71 (2015).
82. A. Ballarino and R. Flukiger, "Status of MgB<sub>2</sub> wire and cable applications in Europe," *J. Phys.: IOP Conf. Ser.* **871**, 1–8 (2017).
83. Y. Iwasa, "Towards liquid-helium-free, persistent-mode MgB<sub>2</sub> MRI magnets: FBML experience," *Supercond. Sci. Technol.* **30**, 0530001(13) (2017).
84. J. V. Minervini, M. Parizh, and M. Schipper, "Recent advances in superconducting magnets for MRI and hadron radiotherapy: an introduction to "Focus on superconducting magnets for hadron therapy and MRI",", *Supercond. Sci. Technol.* **31**, 030301(3) (2018).
85. K. Maekawa, M. Takeda, T. Hamaura, K. Suzuki, Y. Matsuno, S. Fujikawa, and H. Kumakura, "Dynamic level-detecting characteristics of external-heating-type MgB<sub>2</sub> liquid hydrogen level sensors under liquid level oscillation and its application to sloshing measurement," *IEEE Trans. Appl. Supercond.* **27**, No. 4, 1–4 (2016).
86. K. Maekawa, M. Takeda, T. Hamaura, K. Suzuki, Y. Miyake, Y. Matsuno, S. Fujikawa, and H. Kumakura, "First experiment on liquid hydrogen transportation by ship inside Osaka bay," *IOP Conf. Ser.: Mater. Sci. Eng.* **278**, 012066, 1–8 (2017).
87. V. V. Kostyuk, I. V. Antyukhov, E. V. Blagov, V. S. Vysotskii, B. I. Katargin, A. A. Nosov, S. S. Fetisov, and V. P. Firsov, "Experimental hybrid power transmission line with liquid hydrogen and MgB<sub>2</sub>-based superconducting cable," *Tech. Phys. Lett.* **38**, 279–282 (2012).

88. R. Musenich, V. Calvelli, S. Farinon, W. J. Burger, and R. Battiston, "Space radiation superconducting shields," *IOP J. Phys.: Conf. Ser.* **507**, 032033 (2014).
89. R. Bruce and B. Baudouy, "Cryogenic design of a large superconducting magnet for astroparticle shielding on deep space travel missions," *Phys. Proc.* **67**, 264–269 (2015).
90. D. Wang, D. Xi, Q. Wang, J. Feng, X. Pan, C. Chen, G. Yan, P. Zhang, and J. Li, "Fabrication of (6 + 1)-Structure Superconducting Cable Based on 30-Core MgB<sub>2</sub> superconducting wire," *IEEE Trans. Appl. Supercond.* **30**, No. 4, 6200205 (2020).
91. K. Konstantopoulou, A. Ballarino, A. Gharib, A. Stimac, M. Garcia Gonzalez, A.T. Perez Fontenla, and M. Sugano, "Electro-mechanical characterization of MgB<sub>2</sub> wires for the Superconducting Link Project at CERN," *Supercond. Sci. Technol.* **29**, 084005(8) (2016).
92. A. Ballarino, "Development of superconducting links for the Large Hadron Collider machine," *Supercond. Sci. Technol.* **27**, 044024(7) (2014).
93. C. E. Bruzek, A. Ballarino, G. Escamez, S. Giannelli, F. Grilli, F. Lesur, A. Marian, and M. Tropeano, "Cable conductor design for the high-power MgB<sub>2</sub> DC superconducting cable project within BEST PATHS," *IEEE Trans. Appl. Supercond.* **30**, No. 4, 1–5 (2017).
94. A. Ballarino, C. E. Bruzek, N. Dittmar, S. Giannelli, W. Goldacker, G. Grasso, F. Grilli, C. Haberstroh, S. Hole, F. Lesur, A. Marian, J. M. Martinez-Val, L. Martini, C. Rubbia, D. Salmieri, F. Schmidt, and M. Tropeano, "The BEST PATHS project on MgB<sub>2</sub> superconducting cables for very high power transmission," *IEEE Trans. Appl. Supercond.* **26**, No. 3, 5401705 (2016).
95. I. M. Abdyukhanov, A. S. Tsapleva, A. V. Borisov, O. A. Krymskaya, M. G. Isaenkova, and D. K. Figurovskii, "Effect of synthesis conditions on the structure and phase composition of magnesium diboride," *Inorg. Mater.: Appl. Res.*, No. 1, 162–167 (2019).
96. E. C. Park, J. H. Shim, K. S. Hwang, S. M. Sung, J. H. Lim, J. Joo, W. N. Kang, and C.-J. Kim, "Fabrication of C doped MgB<sub>2</sub> wire using mixture of in-situ and ex-situ powders," *IEEE Trans. Appl. Supercond.* **19**, No. 3, 2702–2705 (2009).
97. T. Nakane, K. Takahashi, H. Kitaguchi, and H. Kumakura, "Fabrication of Cu-sheathed MgB<sub>2</sub> wire with high J<sub>c</sub>-B performance using a mixture of in-situ and ex-situ PIT techniques," *Phys. C* **469**, 1531–1535 (2009).
98. Y. Shimada, Y. Kubota, S. Hata, K. Ikeda, H. Nakashima, A. Matsumoto, K. Togano, J. Hur, and H. Kumakura, "Microstructure in high-density MgB<sub>2</sub> wires prepared by an internal Mg diffusion method," *IEEE Trans. Appl. Supercond.* **21**, No. 3, 2668–2671 (2011).
99. G. Z. Li, M. D. Sumption, M. A. Susner, Y. Yang, K. M. Reddy, M. A. Rindfleisch, M. J. Tomsic, C. J. Thong, and E. W. Collings, "Critical current density of advanced internal – Mg – diffusion – processed MgB<sub>2</sub> wires," *Supercond. Sci. Technol.* **25**, No. 11, 115023 (2012).
100. P. Alknes, M. Hagner, R. Bjoerstad, C. Scheuerlein, B. Bordini, M. Sugano, J. Hudspeth, and A. Ballarino, "Mechanical properties and strain induced filament degradation of ex-situ and in-situ MgB<sub>2</sub> wires," *IEEE Trans. Appl. Supercond.* **26**, No. 3, 1–5 (2016).
101. M. A. Susner, T. W. Daniels, M. D. Sumption, M. A. Rindfleisch, C. J. Thong, and E. W. Collings, "Drawing induced texture and the evolution of superconductive properties with heat treatment time in powder-in-tube in-situ processed MgB<sub>2</sub> strands," *Supercond. Sci. Technol.* **25**, No. 6, 115002 (2012).
102. M. Bonura and C. Senatore, "Thermal conductivity and stability of commercial MgB<sub>2</sub> conductors," *Supercond. Sci. Technol.* **28**, 115014(9) (2015).
103. S. I. Schlachter, A. Frank, B. Ringsdorf, H. Orschulko, B. Obst, B. Liu, and W. Goldacker, "Suitability of sheath materials for MgB<sub>2</sub> powder-in-tube superconductors," *Phys. C* **445–448**, 777–783 (2006).
104. I. Ahmad and P. M. Sarun, "Temperature-dependent current transfer behavior of Cu- and Fe-sheathed MgB<sub>2</sub> superconducting wires with vanadium barrier," *IEEE Trans. Appl. Supercond.* **30**, No. 8, 6200307 (2020).
105. A. Stenvall, A. Korpela, J. Lehtonen, and R. Mikkonen, "Current transfer length revisited," *Supercond. Sci. Technol.* **20**, 92–99 (2007).
106. M. S. A. Hossain, A. Motaman, S. Barua, D. Patel, M. Mustapic, J. H. Kim, M. Maeda, M. Rindfleisch, M. Tomsic, O. Cicek, T. Melisek, L. Kopera, A. Kario, B. Ringsdorf, B. Runtsch, A. Jung, S. X. Dou, W. Goldacker, and P. Kovac, "The roles of CHPD: superior critical current density and n-value obtained in binary in situ MgB<sub>2</sub> cables," *Supercond. Sci. Technol.* **27**, 095016 (2014).
107. T. P. Krinitsina, E. I. Kuznetsova, Yu. V. Blinova, D. N. Rakov, Yu. N. Belotelova, S. V. Sudareva, M. V. Degtyarev, and E. P. Romanov, "Structure and stability of superconducting core of single-core MgB<sub>2</sub>/Cu,Nb tube composite with a high critical current," *Phys. Met. Metallogr.* **115**, No. 6, 538–546 (2014).
108. M. Sugano, A. Ballarino, B. Bartova, R. Bjoerstad, Scheuerlein, and G. Grasso, "Characterization of Mechanical Properties of MgB<sub>2</sub> Conductor for the Superconducting Link C. Project at CERN," *IEEE Trans. Appl. Supercond.* **25**, No. 3, 4801004 (2015).
109. X. X. Xi, "MgB<sub>2</sub> thin films," *Supercond. Sci. Technol.* **22**, 043001(15) (2009).
110. T. A. Prikhna, A. P. Shapovalov, A. V. Shaternik, M. Eisterer, V. E. Shaternik, and V. V. Kovylyaev, "Structure and properties of oxygen-containing films of magnesium diboride (MgB<sub>2</sub>)," *Metallofiz. Nov. Tekh.* **37**, No. 3, 327–345 (2015).
111. Z. K. Liu, D. G. Schlom, Q. Li, and X. X. Xi, "Thermodynamics of the Mg–B system: implications for the deposition of MgB<sub>2</sub> thin films," *Appl. Phys. Lett.* **78**, No. 23, 3678–3679 (2001).
112. X. H. Zeng, A. Sukiasyan, X. X. Xi, Y. F. Hu, E. Wertz, Li. Qi, W. Tian, H. P. Sun, X. Q. Pan, J. Lettieri, D. G. Schlom, C. O. Brubaker, L. Zi-Kui, and L. Qiang, "Superconducting properties of nanocrystalline MgB<sub>2</sub> thin films made by an in situ annealing

- process,” *Appl. Phys. Lett.* **79**, No. 12, 1840–1842 (2001).
113. W. Dai, V. Ferrando, A. V. Pogrebnikov, R. H. T. Wilke, K. Chen, X. Weng, W. Joan Redwing, Chung Bark, C.-B. Eom, Y. Zhu, P.M. Voyles, D. Rickel, J.B. Betts, C.H. Mielke, A. Gurevich, D.C. Larbalestier, Qi Li, and X. X. Xi, “High-field properties of carbon-doped MgB<sub>2</sub> thin films by hybrid physical-chemical vapor deposition using different carbon sources,” *Supercond. Sci. Technol.* **24**, 125014(12) (2011).
  114. K. S. B. De. Silva, X. Xu, W. X. Li, Y. Zhang, M. Rindfleisch, and M. Tomsic, “Improving superconducting properties of MgB<sub>2</sub> by graphene doping,” *IEEE Trans. Appl. Supercond.* **21**, No. 3, 2686–2689 (2011).
  115. A. Saito, H. Shimakage, A. Kawakami, Z. Wang, K. Kuroda, H. Abe, M. Naito, W. J. Moon, K. Kaneko, M. Mukaida, and S. Ohshima, “XRD and TEM studies of as-grown MgB<sub>2</sub> thin films deposited on r- and c-plane sapphire substrates,” *Phys. C* **412–414**, 1366–1370 (2004).
  116. M. Paranthaman, C. Cantoni, H. Y. Zhai, H. M. Christen, T. Aytug, S. Sathiyamurthy, E. D. Specht, J. R. Thompson, D. H. Lowndes, H. R. Kerchner, and D. K. Christen, “Superconducting MgB<sub>2</sub> films via precursor postprocessing approach,” *Appl. Phys. Lett.* **78**, No. 23, 3669–3671 (2001).
  117. A. Plecenik, L. Satrapinsky, P. Ktis, S. Gazi, S. Befiacka, I. Vavra, and I. Kostic, “MgB<sub>2</sub> superconducting thin films on Si and Al<sub>2</sub>O<sub>3</sub> substrates,” *Phys. C* **363**, 224–230 (2001).
  118. S. F. Wang, Y. B. Zhu, Z. Liu, Y. L. Zhou, Q. Zhang, Z. H. Chen, H. B. Lu, and G. Z. Yang, “Growth of MgB<sub>2</sub> thin films by chemical vapour deposition using B<sub>2</sub>H<sub>6</sub> as a boron source,” *Chin. Physics Lett.* **20**, No. 20, 1356–13588 (2003).
  119. M. Kuhberger, G. Gritzner, K. R. Soppl, H. W. Weber, A. F. Olsen, and T. H. Johansen, “Preparation and characterization of superconducting MgB<sub>2</sub> films on alumina,” *Supercond. Sci. Technol.* **17**, 764–769 (2009).
  120. A. Berenov, Z. Lockman, X. Qi, J.L., MacManus-Driscoll, Y. Bugoslavsky, L.F. Cohen, M.-H. Jo, N. A. Stelmashenko, V. N. Tsaneva, M. Kambara, N. Hari Babu, D. A. Cardwell, and M. G. Blamire, “Growth of strongly biaxially aligned MgB<sub>2</sub> thin films on sapphire by postannealing of amorphous precursors,” *Appl. Phys. Lett.* **79**, No. 24, 4001–4003 (2001).
  121. S. H. Moon, J. H. Yun, H. N. Lee, J. I. Kye, H. G. Kim, W. Chung, and B. Oh, “High critical current densities in superconducting MgB<sub>2</sub> thin films,” *Appl. Phys. Lett.* **78**, No. 15, 2429–2431 (2001).
  122. M. Hanna, S. Wang, A. D. Eck, R. H. T. Wilke, K. Chen, A. Soukiassian, C. -H. Lee, W. Dai, Q. Li, J. M. Redwing, D. G. Schlom, X. X. Xi, and K. Salama, “Clean epitaxial MgB<sub>2</sub> films fabricated by the ex situ annealing of chemical vapour deposition-grown B films in Mg vapour,” *Supercond. Sci. Technol.* **21**, 045005(40) (2008).
  123. J. Kim, R. K. Singh, N. Newman, and J. M. Rowell, “Thermochemistry of MgB<sub>2</sub> thin film synthesis,” *IEEE Trans. Appl. Supercond.* **13**, No. 2, 3238–3241 (2003).
  124. S. N. Ermolov, M. V. Indenbom, A. N. Rossolenko, I. K. Bdikin, L. S. Uspenskaya, N. S. Stepanov, and V. G. Glebovskii, “Superconducting MgB<sub>2</sub> films obtained by magnetron sputtering,” *JETP Lett.* **73**, No. 1, 557–561 (2001).
  125. P. Kus, A. Plecenik, L. Satrapinsky, Y. Xu, and R. Sobolewski, “Superconducting properties of MgB<sub>2</sub> thin films prepared on flexible plastic substrates,” *Appl. Phys. Lett.* **81**, No. 12, 2199–2001 (2002).
  126. G. Grassano, W. Ramadan, V. Ferrando, E. Bellingeri, D. Marr’e, C. Ferdeghini, G. Grasso, M. Putti, P. Manfrinetti, A. Palenzona, and A. Chincarini, “As-grown magnesium diboride superconducting thin films grown by pulsed laser deposition,” *Supercond. Sci. Technol.* **14**, 762–764 (2001).
  127. A. J. M. Van Erven, T. H. Kim, M. Muenzenberg, and J. S. Moodera, “Highly crystallized as-grown smooth and superconducting MgB<sub>2</sub> films by molecular-beam epitaxy,” *Appl. Phys. Lett.* **81**, No. 26, 4982–4984 (2002).
  128. K. Ueda and M. Naito, “As-grown superconducting MgB<sub>2</sub> thin films prepared by molecular beam epitaxy,” *Appl. Phys. Lett.* **79**, No. 13, 2046–2048 (2001).
  129. K. Ueda and M. Naito, “In situ growth of superconducting MgB<sub>2</sub> thin films by molecular beam epitaxy,” *J. Appl. Phys.* **93**, No. 4, 2113–2120 (2003).
  130. W. Jo, M. R. Beasley, and R. H. Hammond, “Anisotropy and critical current density of MgB<sub>2</sub> thin films grown in situ by molecular beam epitaxy,” *IEEE Trans. Appl. Supercond.* **13**, No. 2, 3257–3259 (2003).
  131. R. Schneider, J. Geerk, F. Ratzel, G. Linker, and A. Zaitsev, “In situ synthesis of MgB<sub>2</sub> thin films for tunnel junctions,” *Appl. Phys. Lett.* **85**, No. 22, 5290–5092 (2004).
  132. B. H. Moeckly and W. S. Ruby, “Growth of high-quality large-area MgB<sub>2</sub> thin films by reactive evaporation,” *Supercond. Sci. Technol.* **19**, L21–24 (2006).
  133. X. Zeng, A. V. Pogrebnikov, A. Kotcharov, J. E. Jones, X. X. Xi, M. L. Ysczeke, J. M. Redwing, S. Xu, Q. Li, J. Lettieri, D. G. Schlom, W. Tian, X. Pan, and Z. -K. Liu, “In situ epitaxial MgB<sub>2</sub> thin films for superconducting electronics,” *Nat. Mater.* **1**, No. 1, 35–38 (2002).
  134. M. Naito and K. Ueda, “MgB<sub>2</sub> thin films for superconducting electronics,” *Supercond. Sci. Technol.* **17**, 1–18 (2004).
  135. X. H. Zeng, A. V. Pogrebnikov, M. H. Zhu, X. X. Xi, S. Y. Xu, E. Wertz, Qi. Li, J. M. Redwing, J. Lettieri, V. Vaithyanathan, D. G. Schlom, Zi-Kui. Liu, O. Trithaveesak, and J. Schubert, “Superconducting MgB<sub>2</sub> thin films on silicon carbide substrates by hybrid physical-chemical vapor deposition,” *Appl. Phys. Lett.* **82**, No. 3, 2097–2100 (2003).
  136. W. K. Seong, W. N. Kang, S. J. Oh, J. K. Jung, C. J. Kim, and J. Joo, “Superconducting property of single-crystal like MgB<sub>2</sub> thin film,” *Phys. C* **470**, 1465–1467 (2010).
  137. S. Lee, “Crystal growth of MgB<sub>2</sub>,” *Phys. C* **385**, 31–41 (2003).
  138. A. V. Pogrebnikov, J. M. Redwing, S. Raghavan, V. Vaithyanathan, D. G. Schlom, S. Y. Xu, Qi. Li, D. A. Tenne, A. Soukiassian, X. X. Xi, M. D. Jo-

- hannes, D. Kasinathan, W. E. Pickett, J. S. Wu, and J. C. H. Spence, "Enhancement of superconducting transition temperature in  $\text{MgB}_2$  by strain-induced bond-stretching mode softening," *Phys. Rev. Lett.* **93**, 147006(3) (2004).
139. D. R. Lamborn, R. H. T. Wilke, Q. Li, X. X. Xi, D. W. Snyder, and J. M. Redwing, "Growth of thick  $\text{MgB}_2$  films by impinging-jet hybrid physical-chemical vapor deposition," *Adv. Mater.* **20**, 319–323 (2004).
140. K. Chen, M. Veldhorst, C. H. Lee, D. R. Lamborn, R. DeFraen, J. M. Redwing, Q. Li, and X. X. Xi, "Properties of  $\text{MgB}_2$  films grown at various temperatures by hybrid physical chemical vapour deposition," *Supercond. Sci. Technol.* **21**, 095015(5) (2008).
141. S. G. Jung, N. H. Lee, W. K. Seong, W. N. Kang, E. M. Choi, and S. I. Lee, "Growth of  $\text{MgB}_2$  thin films by using a novel laser-assisted chemical vapor deposition technique," *Supercond. Sci. Technol.* **21**, 085017 (2008).
142. C. Zhang, Y. Wang, D. Wang, Y. Zhang, Q. R. Feng, and Z. Z. Gan, "Hybrid physical-chemical vapor deposition of ultrathin  $\text{MgB}_2$  films on  $\text{MgO}$  substrate with high TC and  $J_c$ ," *IEEE Trans. Appl. Supercond.* **23**, No. 3, 7500204(4) (2013).
143. C. G. Zhuang, S. Meng, C. Y. Zhang, Q. R. Feng, Z. Z. Gan, H. Yang, Y. Jia, H. H. Wen, and X. X. Xi, "Ultrahigh current-carrying capability in clean  $\text{MgB}_2$  film," *J. Appl. Phys.* **104**, 013924 (2008).
144. K. Onar, Y. Balci, and M. E. Yakinci, "Effect of grain size on the electrical and magnetic properties of  $\text{MgB}_2$  thick films deposited on the  $\text{Al}_2\text{O}_3$  single crystal substrates," *J. Mater. Sci.: Mater. Electron.* **25**, 2104–2110 (2014).
145. J. Chen, V. Ferrando, P. Orgiani, A. V. Pogrebnyakov, R. H. T. Wilke, J. B. Betts, C. H. Mielke, J. M. Redwing, X. X. Xi, and Q. Li, "Enhancement of flux pinning and high-field critical current density in carbon alloyed  $\text{MgB}_2$  thin films," *Phys. Rev.* **74**, 174511(5) (2006).
146. Y. Zhu, D. C. Larbalestier, P. M. Voyles, A. V. Pogrebnyakov, X. X. Xi, and J. M. Redwing, "Nanoscale disorder in high critical field, carbon-doped  $\text{MgB}_2$  hybrid physicalchemical vapor deposition thin films," *Appl. Phys. Lett.* **91**, 082513 (2007).
147. X. X. Xi, A. V. Pogrebnyakov, X. H. Zeng, J. M. Redwing, S. Y. Xu, Qi. Li, Zi-Kui. Liu, J. Lettieri, V. Vaithyanathan, D. G. Schlom, H. M. Christen, H. Y. Zhai, and A. Goyal, "Progress in the deposition of  $\text{MgB}_2$  thin films," *Supercond. Sci. Technol.* **17**, 196–201 (2007).
148. G. Carapella, N. Martucciello, G. Costabile, C. Ferdeghini, V. Ferrando, and G. Grassano, "Josephson effect in  $\text{Nb}/\text{Al}_2\text{O}_3/\text{Al}/\text{MgB}_2$  large-area thin-film heterostructures," *Appl. Phys. Lett.* **80**, No. 16, 2949–2951 (2002).
149. A. Saito, A. Kawakami, H. Shimakage, H. Terai, and Z. Wang, "Fabrication of Josephson junctions with as-grown  $\text{MgB}_2$  thin films," *IEEE Trans. Appl. Supercond.* **13**, 1067–1070 (2003).
150. T. H. Kim and J. S. Moodera, "Demonstration of all in situ magnesium diboride superconductor thin-film tunnel junctions," *Appl. Phys. Lett.* **85**, No. 3, 434–436 (2004).
151. J. Geerk, R. Schneider, G. Linker, A. G. Zaitsev, R. Heid, K. P. Bohnen, and H. V. Lohneysen, "Observation of interband pairing interaction in a two-band superconductor:  $\text{MgB}_2$ ," *Phys. Rev. Lett.* **94**, 227005(4) (2005).
152. A. Brinkman, D. Veldhuis, D. Mijatovic, G. Rijnders, D. H. A. Blank, H. Hilgenkamp, and H. Rogalla, "Superconducting quantum interference devices (SQUIDs) based on  $\text{MgB}_2$  nanobridges," *Appl. Phys. Lett.* **79**, No. 15, 2420–2422 (2001).
153. D. Mijatovic, A. Brinkman, D. Veldhuis, H. Hilgenkamp, H. Rogalla, G. Rijnders, D. H. A. Blank, A. V. Pogrebnyakov, J. M. Redwing, S. Y. Xu, Q. Li, and X. X. Xi, "SQUID magnetometer operating at 37 K based on nanobridges in epitaxial  $\text{MgB}_2$  thin films," *Appl. Phys. Lett.* **87**, 192505(3) (2005).
154. H. Sosiati, S. Hata, T. Doi, A. Matsumoto, H. Kitaguchi, and H. Nakashima, "Nanostructure characterization of Ni and B layers as artificial pinning centers in multilayered  $\text{MgB}_2/\text{Ni}$  and  $\text{MgB}_2/\text{B}$  superconducting thin films," *Phys. C* **488**, 1–8 (2013).
155. R. Russo, "Quality measurement of niobium thin films for Nb/Cu superconducting RF cavities," *Meas. Sci. Technol.* **18**, 2299–2313 (2007).
156. T. Tajima, A. Canabal, Y. Zhao, A. Romanenko, B. H. Moeckly, C. D. Nantista, S. Tantawi, L. Phillips, Y. Iwashita, and I.E. Campisi, " $\text{MgB}_2$  for application to RF cavities for accelerators," *IEEE Trans. Appl. Supercond.* **17**, No. 2, 1330–1333 (2007).
157. C. Zhuang, T. Tan, A. Krick, Q. Lei, K. Xi, and X. X. Chen, " $\text{MgB}_2$  thin films on metal substrates for superconducting RF cavity applications," *Superconductor Novel Magn.* **26**, 1563–1568 (2013).
158. H. Shimakage, M. Tatsumi, and Z. Wang, "Ultrathin  $\text{MgB}_2$  films fabricated by the coevaporation method at high Mg evaporation rates," *Supercond. Sci. Technol.* **21**, 095009(4) (2008).
159. Y. Zhang, Z. Lin, Q. Dai, D. Li, Y. Wang, Y. Zhang, Y. Wang, and Q. Feng, "Ultrathin  $\text{MgB}_2$  films fabricated on  $\text{Al}_2\text{O}_3$  substrate by hybrid physical-chemical vapor deposition with high  $T_c$  and  $J_c$ ," *Supercond. Sci. Technol.* **24**, 015013(4) (2008).
160. H. Shimakage and Z. Wang, "Fabrication of superconducting nanowires using  $\text{MgB}_2$  thin films," *IEEE Trans. Appl. Supercond.* **23**, No. 3, 2200104 (2013).
161. C. Zhang, D. Wang, Z. H. Liu, Y. Zhang, P. Ma, Q. R. Feng, Y. Wang, and Z. Z. Gan, "Fabrication of superconducting nanowires from ultrathin  $\text{MgB}_2$  films via focused ion beam milling," *AIP Adv.* **5**, 027139(8) (2015).
162. S. Fabretti, P. Thomas, M. Meinert, I. M. Imort, and A. Thomas, "Fabrication of Superconducting  $\text{MgB}_2$  Thin Films by Magnetron co-Sputtering on (001)  $\text{MgO}$  Substrates," *J. Supercond. Novel Magn.* **26**, 1879–1882 (2013).

*Translated by N. Kolchugina*